NASA CONTRACTOR REPORT

NASA CR-2838

SIMULATION MODEL OF EROSION AND DEPOSITION ON A BARCHAN DUNE

Alan D. Howard, Jeffrey B. Morton,
Mohamed Gal-el-Hak, and Deborah B. Pierce

Prepared by
UNIVERSITY OF VIRGINIA
Charlottesville, Va. 22903
for NASA Headquarters

NATIONAL AERONAUTICS AND SPACE ADMINISTRATION • WASHINGTON, D. C. • APRIL 1977

1. Report No.	2. Government Accession No.	3. Recipient's Catalog No.
NASA CR-2838		

4. Title and Subtitle	5. Report Date
SIMULATION MODEL OF EROSION AND DEPOSITION ON A BARCHAN DUNE	April 1977
	6. Performing Organization Code

7. Author(s)	8. Performing Organization Report No.
Alan D. Howard, Jeffrey B. Morton, Mohamed Gad-el-Hak, Deborah B. Pierce	
	10. Work Unit No.

9. Performing Organization Name and Address	11. Contract or Grant No.
University of Virginia Charlottesville, Virginia 22903	NGR 47-005-172
	13. Type of Report and Period Covered
12. Sponsoring Agency Name and Address	Contractor Report
NATIONAL AERONAUTICS AND SPACE ADMINISTRATION WASHINGTON, D.C. 20546	14. Sponsoring Agency Code
	SL

15. Supplementary Notes

16. Abstract Erosion and deposition over a barchan dune near the Salton Sea, California, is modeled by bookkeeping the quantity of sand in saltation following streamlines of transport. Field observations of near-surface wind velocity and direction plus supplemental measurements of the velocity distribution over a scale model of the dune are combined as input to Bagnold-type sand-transport formulas corrected for slope effects. A unidirectional wind is assumed. The resulting patterns of erosion and deposition compare closely with those observed in the field and those predicted by the assumption of equilibrium (downwind translation of the dune without change in size or geometry). Discrepancies between the simulated results and the observed or predicted erosional patterns appear to be largely due to natural fluctuations in the wind direction. Although the model includes a provision for a lag in response of the transport rate to downwind changes in applied sheer stress, the best results are obtained when no delay is assumed.

The shape of barchan dunes is a function of grain size, velocity, degree of saturation of the oncoming flow, and the variability in the direction of the oncoming wind. The size of the barchans may be controlled by natural atmospheric scales, by the age of the dunes, or by the upwind roughness. The upwind roughness can be controlled by fixed elements or by sand in the saltation. In the latter case, dune scale is determined by grain size and wind velocity.

17. Key Words (Suggested by Author(s))	18. Distribution Statement
Dunes Wind erosion Wind velocity Wind direction Velocity Measurement	Unclassified - Unlimited Cat. 47

19. Security Classif. (of this report)	20. Security Classif. (of this page)	21. No. of Pages	22. Price*
Unclassified	unclassified	82	$5.00

* For sale by the National Technical Information Service, Springfield, Virginia 22161

ABSTRACT

Erosion and deposition over a barchan dune near the Salton Sea, California, is modeled by bookkeeping the quantity of sand in saltation following streamlines of transport. Field observations of near-surface wind velocity and direction plus supplemental measurements of the velocity distribution over a scale model of the dune are combined as input to Bagnold-type sand-transport formulas corrected for slope effects. A unidirectional wind is assumed. The resulting patterns of erosion and deposition compare closely with those observed in the field and those predicted by the assumption of equilibrium (downwind translation of the dune without change in size or geometry). Discrepancies between the simulated results and the observed or predicted erosional patterns appear to be largely due to natural fluctuation in the wind direction. Although the model includes a provision for a lag in response of the transport rate to downwind changes in applied shear stress, the best results are obtained when no delay is assumed.

The shape of barchan dunes is a function of grain size, velocity, degree of saturation of the oncoming flow, and the variability in the direction of the oncoming wind. The size of barchans may be controlled by natural atmospheric scales, by the age of the dune, or by the upwind roughness. The upwind roughness can be controlled by fixed elements or by the sand in saltation. In the latter case, dune scale is determined by grain size and wind velocity.

INTRODUCTION

The barchan is the simplest transverse dune occurring in isolation on flat terrain with a partial sand cover. Transverse dune complexes in areas of unidirectional wind appear to be coalesced barchanoid dunes. Barchans form under a regime of strong winds blowing from a nearly constant direction (Smith,1970, p.24), and are remarkable in that they preserve their form and size while migrating over long distances downwind (Long and Sharp, 1964; Hastenrath, 1967). Despite a voluminous descriptive literature and a few quantitative measurements of form, rate of migration, and sedimentary texture, a quantitative explanation of the geometry, size, and self-preserving nature of transverse dunes is still lacking.

Because of its simple form (Fig. 1) and the ease of measurements made in the field, the barchan dune affords an ideal starting point for examining the sedimentary processes causing transverse dunes in air or water. The approach reported here involves modelling of the sediment budget of a natural barchan. Observations of wind shear and direction of surface wind over the dune are coupled with sand-transport relationships of the Bagnold type, corrected for the effects of surface slope on the quantity and mean direction of transport, to predict the pattern of erosion and deposition on the dune. This pattern is compared with that implied by self-preservation of form during downwind translation. Rates of erosion or deposition are predicted by following the changes in sediment transport capacity that occur along assumed streamlines of transport (Fig. 2). In moving a distance ∂x downwind both the distance between streamlines, l, and the sediment transport capacity, q (measured in mass of sand transported per unit of time per unit width), will in general change. Changes in

sediment discharge occur because of changes in surface shear stress and because of change in inclination and orientation of the slope relative to the oncoming wind. The rate of erosion over the interval ∂x is given by:

$$\frac{\partial h}{\partial t} = \frac{2(q_1 l_1 - q_2 l_2)}{\gamma(l_1 + l_2)\partial x} = -\frac{1}{\gamma}\left(\frac{q}{l}\frac{\partial l}{\partial x} + \frac{\partial q}{\partial x}\right), \qquad (1)$$

where the second expression is the governing differential equation, the subscripts $_1$ and $_2$ refer to the positions at the upwind and downwind ends of the interval, ∂x, respectively, and γ is the bulk density of the sand. A similar equation was derived for largescale sandflow by Wilson (1971, p. 194). Erosion may therefore occur either by divergence of transport streamlines or from increase in sediment transport capacity in a downstream direction.

This study provides answers to many basic questions about dune processes, including the following:

1. Are Bagnold-type transport relationships adequate to predict sediment discharge on the sloping surfaces of a dune where flow velocities change rapidly downwind?

2. In view of the non-logarithmic velocity profiles over dunes, can measurements of wind velocity near the sand surface yield the shear stress felt by the sand in transport?

3. Do downwind changes in the surface shear cause immediate changes in sand transport, or is there a time (distance) lag?

4. Do changes in assumed grain size or wind velocity alter the simulated pattern or erosion and deposition?

5. How will a barchan respond to a change in wind direction?

EQUILIBRIUM OF BARCHANS

The Stoss Side

In the discussion of self-preservation of form during downwind translation a unidirectional wind is assumed, even though the observed dunes were subject to somewhat variable wind directions as discussed below. Self-preservation of form (i.e., equilibrium), requires that the rate of translation in the direction of the oncoming wind (the oncoming wind is defined as the direction of the undisturbed unidirectional wind, as compared to the topographically-deflected local wind near the surface of the dune) is constant on all parts of the dune. As Figure 3 (A & B) illustrates, the rate of change in surface elevation, $\frac{\partial h}{\partial t}$, for a given rate of downwind migration $\frac{\partial x}{\partial t}$ is related to the slope angle, θ, and to the angle between the oncoming wind and the contour strike, η, by the following (Allen, 1968, p. 100-101):

$$\frac{\partial h}{\partial t} = \frac{\partial x}{\partial t} \text{ Sin } \eta \text{ Tan } \theta \qquad (2)$$

The Leeside

The equilibrium of the lee, or slip face is likewise governed by Equation 2. However, on the higher portions of the slip face most of the saltation and creep load is deposited near the brink and is redeposited over the slip face by repeated avalanching. The assumption of avalanche redistribution allows the treatment of slipface equilibrium by specification of the equilibrium of the brinkline, which is generally a line of separation of the flow, dividing the normal downwind flow on the stoss-side from reverse circulation on the lee face (Coursin, 1964). Analogous to the stoss-side equilibrium, the consequence of self-preservation under

a unidirectional wind is that the rate of translation of the crest in the direction of the wind is uniform at all points of the brinkline, and that the brink height is constant through time. Figure 3C shows that the volume rate of sediment delivery per unit length of brink is given by:

$$\frac{q}{\gamma} \text{ Sin } (\zeta - \omega),$$

where ζ is the angle between the oncoming wind and the brinkline and ω is the angle between the transport direction and the oncoming wind. The volumetric rate of addition to the slip face per unit brink length is:

$$H \frac{\partial y}{\partial t}$$

where $\frac{\partial y}{\partial t}$ is the rate of movement of the brinkline perpendicular to the brink and H is the height of the brinkline above the toe of the dune. However, because of curvature, the brink height must be replaced by an "effective height" H_e, as indicated in Figure 3D. At equilibrium the above quantities are equal:

$$H_e \frac{\partial y}{\partial t} = H_e \frac{\partial x}{\partial t} \text{ Sin } \zeta = \frac{q}{\gamma} \text{ Sin } (\zeta - \omega), \text{ or,}$$

$$q = K\gamma \frac{H_e \text{ Sin } \zeta}{\text{Sin } (\zeta - \omega)} \qquad (3)$$

where $K = \frac{\partial x}{\partial t}$, a constant on all parts of the brinkline.

EQUATIONS OF SEDIMENT TRANSPORT

The relationships between the rate of sediment transport and the wind shear has been summarized in several sets of equations derived from extensive field and laboratory experiments. Because of the interaction between the saltating grains and the near-surface wind, the velocity distribution

near the ground on a flat, naturally rippled sand surface is modified, when sand is on motion from the usual logarithmic profile by the addition of a constant, U_t (Bagnold, 1941, p. 61; Zingg, 1953, p. 121):

$$v(z) = \frac{v_*}{\kappa} \text{Ln} \left(\frac{z}{k}\right) + U_t \quad , \tag{4}$$

where κ is Von Karman's constant, k is a reference height, U_t is the velocity at the threshold of motion at z=k, and v_* is the shear velocity. The apparent roughness length in saltation, z_{0a}, is not independent of the wind strength. Equation 4 plots linearly on semi-logarithmic paper, so that the profile for a given wind shear can also be described by:

$$v(z) = \frac{v_*}{\kappa} \text{Ln} \left(\frac{z}{z_{0a}} \right) \tag{5}$$

where:

$$z_{0a} = k \, \text{Exp}(-\kappa U_t / v_*) \tag{6}$$

The best-known transport formula was developed by Bagnold (1941, p.66):

$$q = C \sqrt{\left(\frac{d}{D}\right)} \frac{\rho}{g} v_*^3 \quad , \tag{7}$$

where, ρ is the fluid density, d is the grain diameter and D is the reference grain diameter (.25 mm in Bagnold's experiments), and C is a constant with a value of about 1.8 for naturally graded sand. Thus estimation of sediment discharge requires determination of the shear velocity. This can done by measurement of wind velocity at one or more heights above the sand surface, assuming Equation 4 to be valid. This approach has been used in the present model.

Other empirical studies have summarized their results with transport

formulas nearly identical to Equation 5 (Zingg, 1953, p. 128; Williams, 1964, p. 280). Formulas of this form are unrealistic in that they predict a small transport rate for shear velocities below the threshold of motion. To remedy this, Lettau and Lettau (in press) have proposed a formula that includes the critical shear stress at the initiation of motion, v_{*t}:

$$q = \begin{cases} C' \sqrt{\frac{d}{D}} \frac{\rho}{g} (v_* - v_{*t})\, v_*^2 & v_* > v_{*t} \\ 0 & v_* \leq v_{*t} \end{cases} \qquad (8)$$

Transport rates predicted by this formula differ from the Bagnold equation only at wind velocities very close to the threshold of motion. A similar equation is implied in later theoretical work by Bagnold (1956, p.294):

$$q = \begin{cases} C'' \sqrt{\frac{d}{D}} \frac{\rho}{g} (v_* - v_{*t})^2\, v_* & v_* > v_{*t} \\ 0 & v_* \leq v_{*t} \end{cases} \qquad (9)$$

The shear velocity at the threshold of motion is a function of the grain size, the sediment density, σ, and the dynamic friction angle, α, which is a characteristic of the sediment shape and surface packing. Bagnold's formula for this relationship (1941, p. 86) is adequate for dune sands (Howard, in press), although more complicated formulas taking into account lift and interparticle attraction have been proposed (Chepil and Woodruff, 1963, p. 222-229; Iverson et al., 1976):

$$v_{*t} = B \operatorname{Tan} \alpha \sqrt{\frac{(\sigma - \rho) g d}{\rho}}, \qquad (10)$$

where B is a constant. The threshold velocity and the reference length in Equation 4 may also be functions of grain size. Bagnold (1941, p. 105) suggests that this reference height is independent of grain size, but that

the threshold velocity is not:

$$U_t = E \sqrt{\text{Tan } \alpha \, d} \cdot \text{Ln } (\frac{30}{d})$$

Zingg (1953, p. 121) finds that both k and U_t depend upon grain size:

$$k = 10 \, d$$

$$U_t = 8950 \, d \text{ (dgs units)}$$

For the simulations reported below k was assumed to be constant, but U_t was allowed to vary with grain size at a rate intermediate between the results of Bagnold and Zingg:

$$U_t = F \sqrt{\text{Tan } \alpha \cdot d} \qquad (11)$$

where F is a constant for a given set of units.

Sand transport on dunes is affected by the slope of the surface, being inhibited on the windward slopes and enhanced by a downslope gradient. Unfortunately, no systematic experimental data has been collected for transport on inclined surfaces, so that Equations 7-9 must be corrected for slope by available theory. Slope effects enter directly into the transport equation (Equations 7-9) as a result of the effects of slope on the motion of saltating grains, and indirectly by the effects of slope on the threshold of motion (Equations 10-11). Existing theory and observation seems adequate to account for the effects of slope on threshold velocity, U_t, threshold shear, v_*, and roughness height, k. The threshold shear on a sloping surface can be calculated by replacing Tan α in Equation 10 by a more complicated function of α, the slope angle, θ, and the angle between the local wind and the direction of the normal of the slope, (Howard, in press):

$$v_{*t} = B \frac{(\sigma - \rho) g d}{\rho} \left[\sqrt{\text{Tan}^2 \, \alpha \, \text{Cos}^2 \, \theta - \text{Sin}^2 \, \chi \, \text{Sin}^2 \, \theta} - \text{Cos } \chi \, \text{Sin } \theta \right] \qquad (12)$$

The threshold velocity, U_t, can be similarly corrected:

$$U_t = F\sqrt{d}\ \sqrt{\sqrt{\text{Tan}^2\ \alpha\ \text{Cos}^2\ \theta - \text{Sin}^2\ \chi\ \text{Sin}^2\ \theta}\ -\ \text{Cos}\ \chi\ \text{Sin}\ \theta} \qquad (13)$$

The reference height, k_s, is assumed to be constant.

The direct effects of slope on transport are less certain. From considerations of the general force and energy balance Bagnold (1956, p.294; 1973, p. 482) has suggested that the transport on a sloping surface can be expressed as:

$$q' = \frac{q}{\text{Cos}\ \theta'\ (\text{Tan}\ \alpha + \text{Tan}\ \theta')} \qquad (14)$$

where q' is the sediment transport rate on the sloping surface, q is the equivalent rate on a flat surface (from Equations 7-9), and θ' is the slope of the surface in the direction of transport ($\text{Tan}\ \theta' = \text{Tan}\ \theta\ \text{Cos}\ \chi$). Because of the lack of empirical verification of Equation 14, the degree of sensitivity of the pattern of erosion and deposition predicted by the composite model was tested by simulations employing both the correction for slope effect (Equation 14) and the uncorrected formulas (Equations 7-9).

FIELD OBSERVATIONS

Observations on three barchan dunes in the Salton Sea dune field (previously studied by Long and Sharp,1964; Norris, 1966) during a two-week period in June, 1973 provided the basic data on dune geometry, sand transport, and wind flow over the dunes which were used to construct and verify the simulation model. The various measurements and their relationship to the simulation model are discussed below.

Plane-table Surveys

Topographic maps with a 0.5 meter contour interval were made of three barchans averaging about 6 meters in crest height above the desert surface (Fig. 1). Wooden stakes were driven into the sand at the 40 to 60 survey sites on the stoss side of each dune. The desert surface on which the dunes were superimposed sloped about 1.5 percent to the northeast. This overall slope was subtracted from the measured elevations to prepare contour maps showing surface elevations above an equivalent flat surface. Relief on the desert floor averaged less than 0.5 meter; this variation in topography was ignored in the preparation of the projected contour maps which were used in the wind-tunnel measurements discussed below. One of the three barchans (Barchan #1) received the greatest diversity and intensity of field observations, and was therefore selected to serve as the prototype dune for the simulation model. The original topographic map of Barchan #1 was used to produce maps of surface gradient and azimuth of the slope strikes which provided basic input data for the simulations. The topographic maps also provided data on brinkline azimuth, slip-face height, and curvature of the slip face. Although the contour maps are felt to conform to normal plane-table accuracy, small errors in determination of the slope or strike on the stoss slope are magnified during the simulation of erosion and deposition

rates. The greatest errors probably occurred just upwind of the brinkline, where the contours are strongly curved (see Figure 1). The simulations showed the greatest variance in this region.

Wind and ripple directions

During the period of study sand-blowing west winds occurred on three occasions. Observations were made after two of these winds and during the third. At each of the wooden stakes on the stoss-side both the direction of the near-surface wind (from downwind vortex scour) and the orientation of ripplemarks was measured. The wind directions indicated by the scour troughs during a strong wind were compared to the direction of air movement indicated by smoke bombs located nearby on the dune surface. The scour troughs proved to be reliable, unbiased estimators of wind direction. These observations were used to construct maps of inferred streamlines of transport of sand across the stoss-slopes of the dune.

Observations of flow and ripple directions over the dune were made following a windstorm from N81W and during a strong wind from S73W. Measurements from aerial photographs of the orientation of the dark, sand-free tails extending from the center of the barchans suggest a mean transporting wind from S82W, that is between the two sets of observations. The majority of the wind-tunnel observations were made with the wind oriented to come from S82W. Because no field observations were made for such a wind, the observations made for wind from N81W and S73W were combined to make a composite streamline map for S82W. The procedure was as follows:

1. The local wind measured at each stake was re-expressed as a deviation (positive or negative) from the oncoming wind for that set of observations. For the oncoming wind of S82W, the deviations were assumed to lie proportionally between the deviation values for the two sets of observations.

2. The calculated composite deviations were used to make a contour map of deviations of the local wind from the oncoming wind from S82W.

3. The deviation contours were translated into a dense pattern of short streamline segments, which were selectively connected to form the streamline pattern shown in Figure 2A.

However, this technique could not be used upwind from the leading edge of the dune, where field observations were absent. The stakes also failed to yield scour marks on the three-dimensional granule ripples covering the upwind toe of the prototype dune. In these areas laboratory measurements of wind direction were made with crossed 45 degree hotwire probes (Gad-el-Hak et al., 1976, p. 48-49). The streamlines are probably less accurate in this region because of the difficulty of making the precise orientation and calibration necessary to use the method. Nevertheless, the streamline map resulting from the combined field and laboratory measurements was internally consistent and very similar in pattern to the surface flow patterns obtained by Allen (1968, p. 307-313) on model barchans in a water flume.

We also attempted to obtain streamlines in the laboratory by emplacing numerous small tufts on the model dune and photographing it during a strong wind. However, the tufts oscillated in the wind, necessitating the averaging of the results of several pictures. The tufts also had a tendency to stick to the surface of the dune and some had a directional bias due to their orientation at the point of attachment. The streamline pattern resulting from the tuft pictures was similar to that obtained by the field measurements except that the tuft pictures indicated less strong deflections of the oncoming wind by the dune. This difference is due to the height of the tufts above the surface. The tufts extended to

about 2.5 mm above the surface during the wind, equivalent to a scale height of about 80 cms. above the prototype dune. Measurements by crossed 45-degree hotwire probes indicate that the deflection of the wind by the dune decreases rapidly with height (Fig. 14), explaining the less marked deflections of the tufts.

During strong winds the movement of the saltating grains visible near the sand surface nearly parallels the wind as indicated by the scour troughs behind the wooden stakes, even where the dune surface slopes 15 degrees across the wind. However, the coarser creep load, which is impelled along the surface by wind stress and saltation impacts is deflected downslope from the direction of the wind in proportion to the surface gradient. A quantitative measure of this deflection is afforded by the alignment of ripple crests, which are formed by the creep load. Analysis of the force relationships at the threshold of motion (Howard, in press) indicates that the grain will begin to move at an angle β from the direction of the applied stress (Fig. 3E):

$$\text{Sin } \beta = \frac{\text{Tan } \theta \text{ Sin } \chi}{\text{Tan } \alpha} \qquad (15)$$

where χ is the angle between the direction of dip of the dune surface and the applied stress. The downwind perpendicular to the ripplemark crests on the barchan dunes obey this relationship with the dynamic friction angle, α, equal to 30.5 degrees. Thus the creep load, comprising about one-fourth of the total load moves perpendicular to the ripple crests, and is deflected downslope from the surface wind on a sloping surface (by a maximum of about 35 degrees on the stoss slopes of the Salton Sea barchans). Because the direction of mean transport lies between the surface wind and the ripple mark perpendiculars, simulation of sediment

transport was conducted both with the streamlines based upon the wind and with ripple mark streamlines.

The ripple streamlines were constructed in a manner similar to the surface wind streamlines, using a proportional averaging of the observed deflections from the field observations with oncoming wind from N81W and S73W to infer the ripple directions for the assumed wind from S82W. A check on the consistency of the method was afforded by comparing the deflections predicted from the field measurements of the ripple perpendiculars with the deflections predicted by Equation 15 using the composite streamlines of the surface wind. The two techniques gave comparable results, although the more direct method was given priority in the few cases with discrepant results.

Grain size

The grain size of the saltation and creep load was not systematically sampled over the dune, and most of the simulations assume a uniform grain size. Over most of the dune the height and wavelength of the ripple marks vary only slightly, with the exception of the upwind edge of the stoss side, which was blanketed by three-dimensional granule ripples (Fig. 15). However, because there is no unique relationship between the grain size of the creep load forming ripples and the size of the grains in saltation (Ellwood, Evans & Wilson, 1975), ripple size is not a good index of the effective grain size in transport. The sand arriving from upwind is likely to be uniform in size along the leading edge, and little lateral variation in grain size has been found along the slip face of barchans, where most of the sand in transport is deposited.

Elevation changes

During the initial survey of the three Salton Sea dunes the height of exposure of each stake was recorded. At the close of the two-week period the net burial or erosion at each stake was measured, and the advance of the brinkline was determined (about 1.3 meters). This data on observed erosion and deposition rates can be compared to the rate predicted by self-preservation (Equation 2). For an assumed mean wind from S82W the following relationships between observed values of Δh, η, and θ were determined by regression, with Δx being estimated by the slope of the regression line:

Dune	Regression Equation (Δh, Δx in meters)	R^2	n	Observed Translation (Δx in meters)
Barchan #1	$\Delta h = 1.59 \sin \eta \tan \theta$	.75	63	1.2
Barchan #2	$\Delta h = 1.48 \sin \eta \tan \theta$	.79	47	1.3

(16)

The brinkline has obviously moved less rapidly than the stoss-side of the dune as a whole. However, during the two weeks of observations reverse east winds pushed back the brink by as much as .6 meters while leaving the remainder of the dune virtually unaffected. Although the strong winds from the west quickly restored a normal brinkline, the east winds had a retarding effect on brinkline migration. The observations were made during a period of transition between strong spring westerlies and weak summer easterlies.

Because the local slope orientation is measured relative to an assumed oncoming wind, the regression equation can be estimated for any assumed direction of the oncoming wind. If the dune is near or at equilibrium to a unidirectional wind, the percent of variance explained by the

regression (R^2) should be greatest for the true mean wind. The explained variance was indeed greater for an assumed wind from S82W than for the two observed winds, that is, S73W and N81W. However, the maximum in explained variance is not sharp, so that this short-term observational data is a less reliable estimate of the effective oncoming wind than is the aerial photo interpretation.

The unexplained variance from the regression might come from several sources, including 1) modifications of form by the east winds, 2) errors in estimation of θ and η from the plane-table contour maps, 3) shape changes caused by variation in wind direction, and 4) finite translation of a curved body. However, the high degree of explanation suggests a close approximation to equilibrium during translation of the observed dunes. Both the erosion and deposition rates observed in the field (Fig. 4A) and those predicted by the assumption of equilibrium (Fig. 4B) will be compared with the rates of change of surface elevation simulated by the model.

Wind velocity

Wind speeds were measured at 13 locations on the stoss side and brink (Fig. 5) on and near Barchan #1 during a sandstorm with the average direction of the oncoming wind from S73W and velocities ranging from 9 to 16 meters per second. Velocities were measured by recording cup anemometers at heights of 69 and 230 cms above the dune surface. Two anemometers were moved from site-to-site, while a third remained stationary near the summit of the dune. At each location 5 to 10 minutes of measurements were recorded and calibrated to a common windspeed using data from the stationary anemometer. However, the number of measurement locations was insufficient to allow accurate contours of velocity to be drawn on the dune. The field measurements were used, however, to check the reliability of the

detailed velocity measurements made in the wind tunnel.

During the day of strong winds the direction of the oncoming winds varied through a range of 30 degrees. However, all but two measurements were made within a 15 degree range.

WIND TUNNEL MEASUREMENTS

Because of the paucity of field measurements of velocities over the dune, velocity profiles over a number of points on a model dune were measured in a wind tunnel. In addition, the use of the wind tunnel allowed greater control of speed and direction of the oncoming wind. The wind tunnel utilized is 60 x 60 cms in cross-section, and has a test section about 8 meters in length. The atmospheric boundary layer was modeled by emplacement of grids to generate turbulence and to shape the velocity profile (Kokus, 1975; Gad-el-Hak et al., 1976, p. 31). A logarithmic velocity profile was simulated in the tunnel, a profile characteristic of the atmosphere under neutral convective stability (Lumley and Panofsky, 1964, p. 103). The model dune, geometrically scaled down from Barchan #1 by a factor of 315 (the model is about 2 cms in maximum height and about 30 cms from wingtip to wingtip), was placed on the floor of the tunnel and the surrounding tunnel floor was covered by a sandpaper with aerodynamic roughness matching the roughness height of the simulated boundary layer.

In order to utilize experimental measurements to supplement the field data, the dune and its surroundings should be geometrically similar to the prototype, and the air flow should be dynamically similar. Direct simulation of sandflow over dunes in the wind tunnel was not undertaken

both because of the experimental difficulties of introducing sand in transport and because of the very restrictive scaling requirements for sediment transport at reduced physical scales (Yalin, 1971; Greeley, et al., 1974). Full modeling of both fluid flow and sediment transport at laboratory scales is generally impossible without use of fluids and particles with exotic viscosity and density, respectively. On the other hand, scaling of just the airflow to laboratory dimensions is less difficult.

Geometric similarity

For geometric similarity of the fluid flow, the following parameters must be considered:

H = Height of dune

W = Width of flow

D = Depth of flow

z_0 = Upwind roughness length

z_D = Roughness length of dune surface

Letting primes denote the model parameters, full geometric similarity would be observed between the model and prototype of (Yalin, 1971):

$$R_H = R_W = R_D = R_{z_0} = R_{z_D} ,$$

where

$$R_H = \frac{H}{H'} , \text{ etc.}$$

In addition, the model dune must be geometrically similar to the prototype. However, full geometric scaling was not possible, for the degree of approach to similarity was limited by the size of the wind tunnel, by the minimum size dune over which accurate measurements could be taken, and by

the necessity to maintain a fully rough turbulent flow at the model scale.

Because the influence of the dune upon the flow diminishes with height and lateral distance, W and D may be eliminated as parameters if W/H and D/H are large for both model and prototype. In the field, flow over an isolated barchan is effectively unbounded in width, whereas the model dunes occupied about one-half of the tunnel width. However, observations both in the field and in laboratory simulation of flow over barchans (Allen, 1968, 0. 307-313) indicate that the perturbation of the flow is negligible more than one-half dune width beyond the dune edge. The boundary layers developed by the tunnel walls at the point of measurement are only 8 cms thick. Therefore the lateral boundaries of the tunnel should have little effect upon the flow over the dune.

Recent numerical simulations of turbulent flow over smooth two-dimensional obstacles indicate that the flow disturbance to shear and pressure are felt to approximately 100 times the obstacle height (Taylor and Gent, 1974). For a narrow three-dimensional body this height may be reduced. In the wind tunnel the ceiling is only about 31 times the dune height, so that some distortion of the flow is probable. However, the wine tunnel measurements showed that the influence of the dune on longitudinal velocity is nearly unnoticeable at a height of about 25 cms. Thus the finite width and height of the wind tunnel should not have markedly affected the flow over the model dune.

The selection of a appropriate natural value of the upwind roughness, z_0, and scaling of the roughness to the wind tunnel posed some difficulties. The only available measurement of roughness length in the Salton Sea dune field was from a single profile measured upwind from the dune by three calibrated cup anemometers during a sand-blowing event. This

measurement suggests a value of about 0.1 cm. This value seems consistent with roughness lengths of sand in saltation during desert sandstorms. The field and laboratory measurements of Bagnold (1941), Zingg (1953), Chepil (1945) and Chepil and Milne (1941) can be used to estimate the roughness length of saltating sand using Equation 6. For a typical desert sand of 0.25 mm, k has a value ranging between 0.3 to 1cm, depending upon size grading (Bagnold, 1941, p. 81; Chepil, 1945; Chepil and Milne, 1941) and U_t (functionally related to k) has a corresponding range of 300 to 400 cm/sec. For a moderate sand-blowing wind (1000 cm/sec at a height of 80 cm) the apparent roughness will therefore range (using Equation 6) from .009 to .05 cm, and for a very intense wind (1500 cm/sec at 80 cm) from .04 to 0.2 cm. By comparison, for wind velocities below the saltation threshold the sand surface would have a roughness of only about 0.008 cm. The values of apparent roughness during saltation compare favorably with quoted field measurements.

Thus the prototype roughness length probably lies in the range of .05 to 0.1 cm, which would suggest an equivalent roughness of about 2×10^{-4} cm at the laboratory scale. However, in the wind tunnel the selection of a roughness height was constrained by the necessity to maintain a fully rough turbulent flow (see Reynold's Number discussion, below), which was only possible for wind speeds attainable in the tunnel for roughnesses greater than about .005 cm. A sandpaper with a roughness of .008 cm was selected, giving a laboratory roughness length 40 times larger than true scale modeling. However, several simulations of turbulent flow by Taylor and Gent (1974) suggest that variations in roughness length for flow over two-dimensional obstacles do not affect the magnitude of the shear forces on the body when the measurements are scaled by upwind shear

(see Equation 26). The laboratory measurements of relative velocities and velocity gradients above the dune surface show little systematic bias when compared to the few field measurements (Fig. 6). Therefore the choice of an upwind roughness length for laboratory measurements of shear does not appear to be critical so long as the roughness is much smaller than the dune scale.

Any contrast in the characteristic roughness between the dune and the surrounding desert would affect the near-surface velocity field due to the growth of an internal boundary layer over the dune. The maximum length of air flow from the leading edge to the brink of the prototype dune is about 45 meters. The depth of the flow near the brink of the dune that would be affected by a dune roughness greater than the surrounding desert would be about 3-5 meters (using formulas from Elliot, 1958). However, complete readjustment of near-surface velocities to a change in roughness is limited to a layer about .03 to .1 times as thick as the internal boundary layer (Blom and Wartena, 1969; Rao, Wyngaard and Coté, 1974). The saltation load carried between barchan dunes is undersaturated, for the sand cover is discontinuous. In addition, the shear velocities over the dune are correspondingly higher than over the surrounding desert. Both of these effects would tend to make the apparent roughness over the dune (Equation 6) larger than between dunes.

Laboratory measurements were made of near-surface velocity over the model dune both with the surface roughened by a .3 to .5 mm graded sand (slightly rougher than the tunnel-floor and sandpaper) and with a hydraulically smooth surface. At the crest velocities over the sand-surfaced dune at the lowest relative height of measurement (.254 cm., corresponding to 80 cms. over the natural dune) indicated approximately 6% lower velocities

than for the smooth dune (Fig. 7). The surface effect dies out rapidly with height. No difference in velocities was noticeable between the smooth and roughened dune at a height of .5 cm. Comparison of model measurements with the anemometer readings at selected points over the prototype dune suggests that the appropriate scaling for the relatively rougher natural dune would be approximately a 10% reduction in velocity at the brink for flow over the actual dune at the 80 cm. level as compared to flow over a hydraulically smooth dune. The laboratory measurements have therefore been proportionally reduced as a linear function of distance travelled over the dune (Fig. 6, solid points), leading to an unbiased, but rather variable relationship between the field and laboratory measurements at the same relative locations. This variance may in part result from crude velocity scaling for the contrast in roughness, but it is more likely due to the large natural variance in measurement both in the field and wind tunnel, to the 15 degree range in direction of the oncoming wind during measurements over the prototype dune, and to slight discrepancies in the geometric similarity of the model dune.

Dynamic similarity

The most important fluid flow scaling parameter is the Reynold's Number, involving the length and velocity scales. Two Reynold's Numbers are of potential importance in the air flow over a dune:

$$Re_R = \frac{v_* \, z_0 \, 30}{\nu}$$

$$Re_D = \frac{U \, H}{\nu}$$

where Re_R characterizes the boundary layer generated by the surface roughness, which is assumed to extend through the flow layer influenced by the dune in both the field and laboratory. The dune Reynold's Number Re_D describes the flow-dune interaction. The values of these Reynold's Numbers and their constituent parameters in the field and laboratory are summarized below:

Parameter		Value	
		Field	Laboratory
z_o	Roughness Length (cm)	.1	.008
v_*	Shear Velocity (cm/sec)	85	52
U	Characteristic Velocity (cm/sec)	1500	500
H	Dune Height (cm)	600	1.9
ν	Kinematic Viscosity (cm^2/sec)	.15	.15
$Re_R = \frac{v_* z_o 30}{\nu}$		1.7×10^3	83
$Re_D = \frac{U H}{\nu}$		6×10^6	6×10^3

Because the roughness Reynold's Number is larger than 70 for model and prototype, the flow is rough turbulent and the fully developed boundary layer is characterized by a logarithmic velocity profile (Schlichting, 1968, p. 578-589). Under these circumstances, preservation of Reynold's Number between the model and prototype is not necessary for dynamic similarity. However, the wind tunnel roughness is very near the limit for fully rough flow; as noted above this prevented the simultaneous satisfaction of geometric similarity of roughness and of dune dimensions.

The high Reynold's Numbers for the flow suggest that values of v/v_* measured at any given point above the dune should be independent of variations in the average velocity of flow. This was confirmed by measurements of velocity profiles over a few points on the model dune at speeds ranging from 5 to 10 meters per second. However, for a natural dune, this may not be true of points close to the dune surface, where the wind profile is affected by the saltating grains; Equation 6 indicates that the apparent roughness, z_{0a}, is a function of v_*, so that the roughness of the dune and the upwind desert changes with flow velocity. If the roughness of the dune and the desert are both largely determined by the roughness of saltation rather than by fixed elements, then the relative roughness of the dune and desert should not change with v_*. Since this is likely to be the case, the simulations of Taylor and Gent (1974) suggest that the natural variation of z_{0a} with v_* should not affect relative velocities over the dune when scaled by v_*.

THE SIMULATION MODEL

Erosion and deposition on stoss-side

The stoss-side simulation entails the estimation of erosion or deposition rates at intervals of approximately 3 meters (prototype scale) along the assumed paths of sediment transport from the leading edge to the brink (Fig. 2). The streamlines are broken into cells, and erosion and deposition within each cell is calculated using Equation 1, which requires estimates of the sediment discharge, q, entering and leaving the cell and of the divergence of the sediment flow, $\frac{q}{l}\frac{\partial l}{\partial x}$. The flow divergence, $\frac{\partial l}{\partial x}$, was measured directly by the widths of the upstream and downstream ends of the cell (l_1 and l_2, respectively), so that:

$$\frac{\partial l}{\partial x} = \frac{l_2 - l_1}{x} \tag{17}$$

where x is the cell length in the direction of the wind. For the small values of divergence occurring on the dune, the divergence can also be estimated from a contour map of the angular deviation of the surface wind from the oncoming wind, where the angle of deviation was read for the four corners of each cell, the divergence being given by:

$$\frac{\partial l}{\partial x} = \frac{\psi_{ur} + \psi_{dr} - \psi_{ul} - \psi_{dl}}{2} \tag{18}$$

where the local wind deviation, ψ, is measured in radians and the subscripts refer to upstream, u, downstream, d, left, l, and right, r (viewing downstream). The latter estimate of divergence was found to give the same average values as the former, but resulted in a lower variation in estimates from cell-to-cell. The angular method is therefore more

accurate, and was used for the simulations.

The local transport rate, q, was estimated at the upstream and downstream ends of each cell, which requires the specification of several parameters. The angular relationships, θ, ψ and χ varied over the dune and were evaluated for each cell end by the use of contour maps of these quantities. The constants B, D, F, and C, (or C' or C") as well as the sediment and fluid density, σ and ρ, and the dynamic friction angle, α, were given fixed values (Table 1). The grain size, d, was specified as an input variable, and was usually assumed to be constant over the dune. The shear velocity, v_*, was specified by the field and wind tunnel measurements of near-surface velocities over the dune and scaled by an assumed undisturbed upwind velocity $v_0'(z)$. The wind velocities measured in the laboratory at .25 and .5 cms above the dune surface (80 and 160 cms, prototype scale) were scaled with respect to the oncoming wind at the same level, $v_0(z)$, and contour maps of $V(z) = v(z)/v_0(z)$ were prepared for the two heights (Fig. 5).

Two methods were used to calculate the shear velocity, v_*, from the contour maps. The first method assumes that the shear velocity is constant below the lowest level of measurement (80 cm, prototype scale), so that Equation 4 can be used to calculate v_*:

$$v_* = \frac{\kappa(V(80) \cdot v_0'(80) - U_t)}{\ln(80/k)} \tag{19}$$

where $v_0'(80)$ and k are input parameters for the simulations, and U_t was calculated from Equation 13 for the assumed grain size. Simulations of two-dimensional turbulent flow by Taylor and Gent (1974) indicate that the shear velocity is nearly constant to about the relative level, z/H, of the present measurements. Profiles of velocity at the brink of the

dune compare closely with these simulations, and suggest a nearly constant shear stress below the 80 cm level of measurement (prototype scale) (Fig. 7). However, a second method of estimation of v_* was also attempted which fitted a smooth curve through the three points with height coordinates of ln k, ln 80 and ln 160, and respective velocity coordinates of U_t, v(80), and v(160). The shear velocity was estimated from the slope of the curve at the reference height, k:

$$v_* = \kappa \left.\frac{\partial v}{\partial z}\right|_k$$

Formulas for a beam bent through three points (Merrit, 1968) were used to calculate the curve.

In many simulations the discharge at a given point was assumed to be in equilibrium with the shear velocity at that same point, so that Equations 7-9 can be used directly to estimate the discharge at the upstream and downstream ends of each cell. However, some researchers feel that changes in sediment transport lag behind changes in shear stress, and that this lag might, in fact, cause the unstable relationship between sand transport and near-surface wind responsible for the formation of dunes (Bagnold, 1956, p. 294; Kennedy, 1969, p. 154; Reynolds, 1965), whereas Raudkivi (1966) feels no lag is necessary. To test these hypotheses, the actual sediment transport rate at a point, q_a, was assumed to be a weighted function of the equilibrium transport rate at that, q_e, and of the actual transport rates for upwind points. A geometric weighting of upwind actual discharges was adopted:

$$q_{ai} = \frac{q_{e1}}{\lambda + 1} + \sum_{i=2}^{n} \frac{q_{ai}}{\lambda + 1} \cdot \left(\frac{\lambda}{\lambda + 1}\right)^{i-1} \qquad (20)$$

where the subscript i refers to successive upwind streamline cell boundaries relative to the current cell boundary at i=1. The parameter ψ is the average delay; a delay of zero is equivalent to a transport rate in equilibrium with the shear stress. The number of upwind transport rates, n, taken into account was 11 for average delays less than 3 cells (about 9 meters) and 26 for delays up to 10 cells. The weights were adjusted for the finite series of Equation 20 so as to sum to unity. The geometric distribution is a discrete approximation to the exponential, and embodies the following properties which appear to provide a realistic modeling of a lag in transport rate:

1. The transport rate at equilibrium with the shear stress at the given point receives the greatest relative weight.

2. The influence of upwind discharge rates decreases with distance upwind.

3. The actual discharge rate approaches the equilibrium transport rate as a limit following a step change in the equilibrium rate. The rate of adjustment is proportional to the discrepancy between the actual and equilibrium transport rate.

The discharge upwind of the first cell on the dune at the leading edge is assumed to be uniform and equal to the equilibrium transport rate times an assumed value for the percentage saturation for the upwind flow. Thus the actual transport rate at any point on the dune is a function of both the delay constant and of the percentage of initial saturation, P. Both parameters were specified as input to the simulations. In the case of assumed equilibrium transport ($\lambda = 0$), the degree of upwind saturation affects rates of erosion and deposition only at the first cell of each streamline at the leading edge.

Slip-face migration

The simulated rate of translation of the slip face in the direction of the oncoming wind is a function of the sediment discharge at the brink, of the effective slip face height, and of the geometrical relationships at the brink (Equation 3). This rate was evaluated at each streamline lane terminating at the brinkline (Fig. 2).

RESULTS

The product of the simulation model is the distribution of predicted rates of erosion and deposition over the stoss-side and rates of translation of the slip face in the direction of the oncoming wind. These simulated results are to be compared with erosion and deposition rates predicted by the criterion of self-preservation or with the observed rates during the field study. To effect this comparison, the simulated, predicted, and observed rates must be normalized by division by the rate of downwind translation of the dune, so that erosion or deposition is expressed per unit downwind translation of the dune, that is, by $\frac{\partial h}{\partial x}$. Normalized predicted erosion rates are given by dividing both sides of Equation 2 by the translation rate, $\partial x/\partial t$ (Fig. 4B). The observed rates of surface change are normalized by the estimated regression slope of Equation 16(Fig. 4A). The simulated rates can be normalized either by 1) the median of the translation rates estimated at the brinkline terminations of the individual streamline lane or 2) by the average value of the translation rates estimated for each cell by use of Equation 2. The former method was used because it does not presuppose the validity of Equation 2 and because it ties together the brinkline and stoss-side equilibria.

Stoss-side

As with most models of physical processes, the simulation of the sediment budget over the barchan dune will be considered a success to the degree that the predicted patterns of surface changes over the dune agree with either the observed or predicted patterns. The degree of this agreement is assessed by several quantitative measures. The average difference between the simulated erosion and deposition rates and the observed (or predicted) rates for each streamline cell on the stoss-side is termed the bias:

$$\hat{b} = \frac{\sum_{i=1}^{n} (s_i - o_i)}{n} \tag{21}$$

where $\hat{b}$ is the estimated bias, s_i is the simulated rate of change, o_i is the observed (or predicted) rate, and n is the number of streamline cells. The degree of variation is measured by the variance of the differences between the simulated and observed rates, corrected for the bias:

$$\hat{v} = \frac{\sum_{i=1}^{n} (s_i - o_i - \hat{b})^2}{(n - 1)} \quad . \tag{22}$$

Finally, the simulations are compared with expected results through the use of the standard correlation coefficient between s_i and o_i. Of these measures, the bias and variance are affected by the normalization of the simulated erosion rates by the translation of the crest. A low bias and variance will result only if the simulation model 1) reproduces the relative rates of erosion and deposition over the stoss-side and 2) simulates a rate of advance of the brink consistent with the erosion rates on the stoss-side. The correlation coefficient measures only the first of these.

For comparison purposes the bias, variance, and correlation were calculated separately for the initial upwind cells of the streamlines (the leading edge) and for the remaining stoss-side points (the core). This separation was made because the assumed initial undersaturation on the oncoming flow affects only the leading edge cells for those simulations with no assumed lag, λ. Also, the leading edge points were expected to show the greatest deviations between simulated and predicted erosion rates because the streamlines were poorly defined upwind of the leading edge.

These comparative statistics were used to test the effects of variations in the parameters of the simulation model as well as the effects of more fundamental changes in the mathematical structure of the model. Because of the large number of possible variations in the model parameters and model structure, not all combinations could be investigated. Rather, a nominal set of conditions were assumed to which individual model variations could be compared. The nominal variations were selected to represent a grain size (.25 mm) and an undisturbed upwind velocity ($v'_0(80)$ = 1000 cm/sec) that closely approximate the observed conditions on the prototype barchan, and the combination of transport law (modified Bagnold, Eqn. 9), delay (λ=0), transport path (following the wind streamlines) and slope effect (slope effect estimated by Equation 14) that both appears to be physically reasonable and provides a comparatively close simulation of the predicted erosion and deposition rates.

Variation in velocity and grain size

The bias and variance of the core cells was calculated for several sets of model assumptions (discussed below) for the case with zero delay

(λ=0 in Equation 20). When the sand is assumed to follow the wind streamlines the bias and variance show a weak dependence upon wind velocity (Fig. 8A). An increase in wind velocity reduces the small negative bias, and likewise lessens the variance. For transport assumed to follow the ripple train the variance behaves similarly to the wind streamlines, but the bias becomes a strong function of wind speed, changing from negative to positive in the range of wind speeds from 750 to 2000 cm/sec. For leading edge cells the negative bias becomes more pronounced as wind speed increases, whereas the variance shows little dependence upon velocity, except in the case of transport along the ripple train, where it increases with velocity. This pattern of variance and bias is repeated for grain size, but an increase in grain size produces the same effect as a decrease in wind speed (Fig. 8B).

Delay and saturation

If transport rate lags behind local shear stress ($\lambda > 0$) the initial undersaturation becomes distributed among the core cells, so that the bias and variance depend jointly upon the degree of initial saturation and the length of delay. The effects of these parameters were investigated for nominal conditions for delays up to 10 cells (about 32 meters, prototype scale) and for an assumed initial saturation of 50% (Fig. 9). Bias of the leading edge markedly declines in absolute value as the delay is increased from 0 to about 2 cells, but then remains nearly constant for longer delays. The bias of core points is less markedly affected by either delay or saturation with the bias slowly lessening as delays are increased. Variance of the core points declines abruptly from 0 to ½ cell delay, then increases slowly for longer delays. A similar pattern occurs for leading edge cells, but minimum variance

occurs at about a 2-cell delay. The decrease in core variance for short delays is probably due to the averaging effect of the delay function (Equation 20). Similar, but even more marked reductions of variance are effected by contouring the simulated erosion and deposition rates by hand (Fig. 10), which smooths out local variance (Table 2). Neglecting the averaging effect, longer delays thus increase the variance of the simulated results compared to the predicted rates.

The degree of saturation of the sand flow approaching the prototype dune is uncertain. The simulation model affords two indirect methods to determine the saturation required for equilibrium of the dune. One estimate results from determination of the degree of saturation that results in zero average bias for the leading edge cells. An initial saturation of about 80-85% (for nominal conditions and zero delay) is suggested by this criterion. The second approach estimates the amount of sand lost from the wingtips of the dune, summing the discharge from those streamline lanes that do not terminate at the brink. This lost amount is then compared to the percentage of saturation of the oncoming flow that would deliver an equal input of sand. This method gives saturation estimates ranging from 20 - 65%, depending upon how many of the wingtip streamlines lanes are counted as contributing to the sand loss. However, this latter estimate is less reliable, for a small percentage of the finer sand component arriving at the brink is carried over the zone of reverse flow in suspension. Also, the resultant wind direction on the wingtip portions of the slip face is towards the wingtip (Coursin, 1964; Allen, 1968, p. 311; Howard, field observations). A small amount of lateral transport occurs on the wingtip faces, aided by intermittent vortices which migrate downwind along the slip face. These added

contributions to the sand loss suggest that the saturation lies closer to the 80 - 85% estimate.

Slope effect

Simulations were calculated using both slope-corrected transport formulas (Equation 14) and non-corrected formulas (Equation 7-9). Simulations ignoring the slope effect resulted in lower absolute values of the bias and lesser variance than the slope-corrected formulas (Fig. 8).

Transport formula

Simulations were made for the original Bagnold formula (Eqn. 7), the modified Bagnold formula taking into account the critical shear stress (Eqn.9) and the similar Lettau formula (Eqn. 8), All three formulas provided very similar results for high velocities and/or small grain size, but whereas the original Bagnold formula indicated bias and variance nearly independent of grain size and wind velocity, the Lettau and modified Bagnold formulas simulated sharply increased variances and greater negative bias for large grain size and low wind velocity, that is, near the threshold of motion.

Effect of divergence

The effect of neglecting the divergence term in Equation 1 was investigated in one simulation with otherwise nominal conditions. Results with no convergence were not markedly different from results with convergence (Table 2). A greater difference would have been observed for assumed transport following the ripple train, for the streamlines are more strongly bent (compare Figs. 2A and 2B). Changes in surface shear are thus more important in determining stoss-side equilibrium than are the direct effects of sediment convergence and divergence.

Shear stress estimation method

In one simulation the shear stress was estimated by the beam-bending method rather than by the asssumption of constant stress below the level of velocity measurement (Eqn. 4). This simulation, with otherwise nominal condition, resulted in a much higher core variance and bias as compared to those utilizing Equation 4.

Because the rate of erosion or deposition on the stoss-side responds to the rate of change of discharge along the streamline, small errors in the original data are magnified in the predicted results. The stoss-side variance is partially due to these random variations, as well as to systematic deviations between simulated and observed (or predicted) results. In order to suppress the random component, smoothed contour maps of erosion and deposition were constructed by hand for six simulations for nominal velocity, grain size, and transport law, but with different assumptions about transport path, slope effect, delay and presence or absence of convergence effects (Fig. 10). These six simulations were compared not only to predicted erosion rates but also with observed rates. The bias, variance, and correlations statistics indicate, like the previous results, that the best overall agreement with both observed and predicted rates is obtained with zero delay, transport following the wind, slope effects discounted, and with convergence retained (Table 2). The simulated rates agree nearly equally with observed and predicted rates with the exception of the bias, which is closer to zero for the predicted rates.

Because the mean transport path presumably lies between the wind streamlines and the ripple train, the simulated results for the wind and ripple cases were combined by least squares fit to observed and predicted

rates, resulting in marginal improvement of explanatory power (Table 2). The proportion of the ripple train simulation in the least-squares combination varies from 7 to 47 percent, depending upon the combination of simulations and whether the results were compared to the observed or predicted rates. This range encompasses the 20 to 25 percent proportion of the total sandflow moved by surface creep, which appears to follow the ripple train (Howard, in press).

Brinkline

The simulations can also be judged by the degree to which they predict brinkline equilibrium. Values of sediment discharge at the brink terminations of streamline lanes were plotted versus the factor

$$f = \frac{H_c \text{ Sin } \zeta}{\text{Sin } (\zeta - \omega)} \quad .$$

If the simulations predicted a perfect equilibrium, the points would plot on a straight line through the origin with slope dx/dt (Eqn. 3). The resulting plots for most simulations appear to be linear, but with considerable scatter, partially due to data errors and partly due to the failure of the assumptions, particularly the assumption of equilibrium with a unidirectional wind (Fig. 11). The point that falls higher than the general trend (Fig. 11A) is probably due to an overly high velocity estimate at that point on the brink (errors in velocity become cubed during the calculation of discharge). The shape of the plots is essentially insensitive to variation in grain size, in velocity, to the transport law assumed, and to inclusion or exclusion of slope effects and convergence. However, the plots are very sensitive to the assumed transport direction and to the amount of assumed delay. The simulated

results following the wind provide a closer approach to the assumed equilibrium than do the ripple train simulations (Fig. 11(A&B). For delays greater than about 2 cells (6 meters, prototype scale) the points no longer are consistent with a line passing through the origin (Fig. 11C). This is due to a decrease in the difference in discharge between the high central portions of the brink and the lower wings.

Interpretation

Comparison of the observed, predicted, and simulated patterns of erosion and deposition (compare Figs. 4 and 10) reveal that the major discrepancy for assumed transport following both wind and ripple paths is a large underestimate of erosion rates on the stoss-side near the toe. In addition, the ripple path simulations indicate a zone of overly-strong deposition along the wingtips of the dune, due to strong flow convergence. The remaining discrepancies are smaller and generally not symmetrically distributed on the two sides of the dune. Such minor areas of discrepancy might easily have arisen due to slight differences between the geometry of the prototype and model dune (with the resultant effects upon the near-surface windflow) or to local errors in mapping of velocities over the model dune. Non-unidirectional winds probably also play a role in non-symmetrical discrepancies between simulated and observed (or predicted) patterns of erosion and deposition (the slight assymmetry of the dune suggests such influences). The area of major underestimation of erosion rates near the central leading edge is possibly due to several factors.

1) Differences in dune shape between the model and prototype might have produced unrepresentatively low shear stresses in the discrepant area.

2) Flow divergence in the area of question may have been

underestimated, which would reduce simulated erosion rates.

3) The change from desert floor to loose sand just upwind from the zone in question may be associated with a change in saltation mechanics which would lead to local scour. For example, saltation over desert pavement and granule ripples is characterized by large heights of grain rebound (Bagnold, 1941, p. 7; Ellwood, et al., 1975), and hence by high kinetic energy, whereas saltation over ripples composed of sand which is only slightly coarser than the saltating grains is characterized by much lower rebound heights due to a greater energy dissipation upon impact.

4) When the wind during sand transport is not unidirectional, but fluctuates (a range of up to 30 degrees was observed in the field), the hump of the dune along the central line of symmetry will be more strongly eroded than in the case of a unidirectional wind due to the added exposure of the centerline for skewed oncoming winds.

The first three of these potential explanations share a common problem; were the large area of erosional deficit on the central stoss side eliminated by adding additional sand into transport, the required velocities would be much higher than observed, and the quantity of sand in transport would be greater than would be allowed for brinkline equilibrium. These problems can be quantitatively illustrated by running the simulation model backwards, that is, by assuming that the predicted erosion rates actually occur and to calculate the necessary distribution of velocity and sand discharge. Such an approach was taken for several combinations of assumed transport law, presence or absence of direct slope effects, wind versus ripple transport paths, and for various wind velocities and grain sizes. Because of the difficulty of unravelling the effects of

lags between shear stress and sand transport, all simulations were conducted at zero delay. The resulting hypothetical velocity distributions (Fig. 12) are not markedly different than either field or laboratory mesurements of near-surface velocities (Fig. 5; Table 3) except along the center of symmetry of the dune, where very high velocities would be required. Relative to both field and laboratory measurements, the required velocities are so much higher than the observed speeds that explanations 1) and 2), above, are clearly inadequate. The third explanation is also rendered questionable by the large quantity of sand that would of necessity be carried over the central portions of the brink if the dune were in strict equilibrium with unidirectional winds (the required discharge follows directly from along-streamline bookkeeping of changes in transport rate required by Equation 1). A plot of the required sandflow versus the f-factor for brinkline equilibrium illustrates this (Fig. 11D); the striking upturn of the curve at higher values of q and f (along the central portions of the brink) indicate that equilibrium of the stoss-side with unidirectional wind is inconsistent with brinkline equilibrium.

Therefore the form of the prototype barchan appears to be shaped by winds from a range of directions. The observed 30 degree variation in the direction of sand-transporting winds and the assymmetry of the dune support this conclusion. Minor variations in the direction of the oncoming wind can cause large changes in near-surface velocities. Winds arriving at an angle to the direction of symmetry will exert a greater shear on the central stoss due to its greater relative exposure for variable wind. The extra sand eroded from the central stoss would be carried to portions

of the brink along the downwind side of the center, reducing the relative amount of sand flowing over the central brink as compared to that arriving to either side. This redistribution of sand would tend to linearize the relationship shown in Figure 11D.

Accordingly, a barchan dune shaped by a completely unidirectional wind must have a somewhat different form than one shaped by a more varied wind. In particular, the central axis of the stoss side would have to project further upwind, approaching more closely to a canoe shape. The narrow "bow" would increase both the shear and divergence on the central stoss, eliminating the zone of underprediction. The average shear on the lower portions of the two wings would be reduced, compensating for the zones of excess erosion simulated on the wings (Fig. 10).

Despite the systematic discrepancies between simulated and observed (or predicted) erosion and deposition rates due to variations in direction of the oncoming wind, the model sufficiently reproduces the predicted rates that the assumptions of the model appear to be substantially correct. In particular, the following conclusions are suggested:

1) The prototype dune was near equilibrium with a nearly unidirectional wind.

2) Bagnold-type sand transport equations, corrected for slope effect, accurately describe sand transport over dunes. The slightly different equations tested (Equations 7-9) produced only minor variations in predicted patterns of erosion and deposition. Simulations of erosion and deposition rates neglecting the direct effect of slope on transport rates (Eqn. 14) are slightly better than those that include the slope effect (Fig. 8). However, velocity simulations including the slope effect are better (Table 3).

3) Variations in shear over the dune are more important than

convergence and divergence in determining the equilibrium of the dune.

4) A delay between downwind changes in shear stress and the resulting rate of sand transport is not needed in order to account for the equilibrium of the dune, and the predictions of the model are less accurate when long delays are assumed.

5) Measurement of the near-surface velocity distribution over the dune (at a scale height of $z/H = .13$), when combined with Equation 4 gives an accurate measure of the surface shear, except perhaps over sharply curved portions of the stoss.

6) Very similar patterns of erosion and deposition rates are simulated for transport along wind streamlines and along the ripple train, except on the wings where convergence is strong in the ripple case. This indicates that the shear distribution is more important in determining erosion and deposition rates than is the direction of transport. However, the brinkline is closer to equilibrium with wind streamline sandflow than with ripple train flow, suggesting that the bulk of the sand closely follows the wind across the dune.

THE EQUILIBRIUM OF THE BARCHAN

The interactions between the sediment flow and airflow responsible for creation and regulation of barchan dunes will remain partially obscure until the windflow over the dune can be adequately modeled, either numerically or analytically. However, the simulation model illuminates several facets of these interactions. The development of dunes requires both an initial instability in the transport of sand over a level desert surface, leading to an accumulation of sand, and feedback mechanisms between the airflow and sand transport which limit the growth of the

accumulation to a given size and shape of deposit. Bagnold (1941, p. 167-187) felt that the initial instability might arise due to the greater rebound of grains on a desert surface relative to loose sand, allowing oversaturation of sandflow over the desert floor. Irregularities in the desert floor topography may also encourage deposition. Unfortunately, the simulation model offers little evidence regarding the the destabilizing mechanisms.

The feedback mechanisms determining equilibrium are clearer. These interactions are of two types, those that control the shape of the dune, and those that affect the shape. The regulating mechanism controlling the shape are more sensitive than those controlling the size, as suggested by several observations:

1) Slight variations in geometry of the dune relative to the oncoming wind cause major changes in the velocity distribution over the dune, and hence, in the spatial pattern of relative erosion and deposition. The effect upon near-surface velocities of variation in direction of the oncoming wind (Fig. 13) illustrates this effect.

2) When a smaller barchan overtakes a larger, the two often unite as a single large dune similar in shape to the original dunes.

3) Field observations indicate that dune shape responds very rapidly to changes in wind direction. Reversal of wind direction forces a rapid reversal of dune orientation with little change in bulk, and the reorientation occurs after a relatively short distance of migration (Smith, 1970). Major changes in dune size, however, occur only after the dune has migrated a considerable distance downwind.

4) In a given dune field the largest barchans may be more than ten times the size of the smallest, but large and small barchans differ very

little in shape (Finkel, 1959; Coursin, 1964, Hastenrath, 1967).

Dune shape

The factors controlling dune shape will be considered first, and the equilibrium of the stoss slopes will be considered separately from that of the brinkline. The flow over the stoss is little affected by the flow downwind from the brink, because the flow separates at the brink. The barchan is approximately shaped like the chordal section of an ellipsoid of revolution (a "whaleback") with the downwind portion scooped out. The influence of the missing section upon the overall form drag is minor, due to the low shear stress that would exist on the lee side even were the missing portion filled in.

The stoss-side geometry can be roughly characterized by two ratios, H/W and W/L, where H is the crest height, W is the wing-to-wing width transverse to the flow, and L is the distance from the toe of the leading edge to the crest. If H/W were larger than on the prototype barchan (W/L constant), the shear stress on the crest would be increased relative to the basal portion of the dune, the streamlines near the toe would be more divergent, and the steeper gradients would cause a greater downgradient component to the sediment flow, reducing sand delivery to the crest. All these factors cause a more rapid crestal erosion, tending to return the dune to equilibrium. Similarly, if the W/L ratio were increased from its value on the present dune (H/W constant), the shear stress on the central stoss near the toe would be reduced relative to the wings, whereas the wings would be more exposed. Sediment transport over the central toe would lag relative to the wings and crest (due to both reduced shear and steeper upslope gradient), tending to restore equilibrium (although a greater flow divergence would partially counteract

the sheltering of the central leading edge). The overall streamlined shape and the gradual tapering of the height from the center of the dune to the leading edge is due to the very rapid erosion that would occur to any mass of sand that projected sharply into the wind.

The effects of variations of grain size and velocity upon dune shape are indicated by the relative rates of erosion on the basal wings (w areas, Fig. 2A), the central leading edge (1 area), and on the crest (Area h). The average rates of erosion, $\overline{E}_w$, $\overline{E}_h$, and $\overline{E}_1$, were calculated for each simulation for the streamline cells within the respective areas, pooling the w_1 and w_2 areas, so that variations in the ratios $\overline{E}_w/\overline{E}_h$ and $\overline{E}_1/\overline{E}_w$ are indices of predicted variations of H/W and W/L, respectively, that would accompany change in grain size and velocity. These ratios suggest that either an increase in wind speed or a decrease in grain size should cause a moderate increase in H/W and a rapid increase in E/L, that is, the dune would be steeper and more blunt.

Increase in the assumed delay between changes in shear stress and sand transport rate tends to increase H/W and marginally to decrease W/L.

The equilibrium of the brinkline is more complex due to the upwind influence of the separated flow, between changes in brinkline shape and the geometry of the stoss side. The brinkline can adjust to lateral differences in sand supply by changing the curveature of the crest, which affects H_e, by change in orientation relative to the mean wind, which affects the angular relationships on the right-hand-side of Equation 3, and by change in shear stress as the relative position of the brink varies.

Changes in curveature are the most important regulating mechanism near the crest of the barchan. Near-surface velocities drop off very slowly away from the crest (Fig. 5). Therefore, if the brinkline were,

for example, initially straight and perpendicular to the sandflow, the central part would migrate less rapidly than the adjacent lower brinkline which receives nearly the same sand supply but has a lower slip face. The crestal lag would create a concave curvature of the slip face, reducing the area of deposition and speeding up the brink movement. Such a feedback mechanism creates a stable, sharply-curved crestal brinkline.

The orientation of the brinkline on the wings is due to a more complex interaction of the terms in Equation 3. The crestline here is nearly linear, so that curvature is not a factor. These interactions can be illustrated by disturbing the natural brinkline by an incremental forward displacement of the wings relative to the central brink. Comparing points of equal elevation on the displaced and original brinkline the inward curvature of streamlines near the crest implies a decrease in ζ and an increase of ω. Thus the angular terms in Equation 3 imply, other factors being equal, a slight increase in the rate of downwind translation of the brinkline, a destabilizing influence. However, this is overbalanced by the decrease in velocity (and transport rate) that occurs due to the greater sheltering of the advanced brinkline from the wind (on the barchan wings, velocity decreases along the contours as the crest is approached, see Figure 5). Thus a displacement of the crestline on the wings causes a return toward equilibrium.

The position of the brink relative to the leading edge is likewise a function of the sediment budget. A slip face will not be stable unless an overall divergence of sandflow occurs on the stoss edge to compensate for sand supplied from upwind and for the inward convergence of sand avalanching down the slip face. A balance must also, of course, be maintained between interception of sand from upwind and loss from the dune

by streamers from the barchan wing tips (Bagnold, 1941, p. 212, Lettau and Lettau, 1969).

The factors controlling the position of the brink relative to the leading edge of the dune can be illustrated by first considering the equilibrium of a two-dimensional dune transverse to the flow. Equations 1 and 2 imply for a two-dimensional dune at equilibrium that

$$\frac{1}{\gamma}\frac{\partial q}{\partial h} = \frac{\partial x}{\partial t} = K, \text{ or } \frac{q}{\gamma} = K\,h + q_0, \tag{23}$$

where K is a constant for the given dune. However, a slip face with its brink at a given height, h, must migrate forward at a rate $K' = \frac{q}{\gamma h}$. Thus a slip face on a two-dimensional transverse dune is unstable, for it will always migrate forward faster than the dune as a whole. However, on a barchan, the sandflow diverges as it crosses the stoss-side, gradually reducing K' downstream so that at some point a brink can exist in equilibrium with the stoss-side migration rate. As an example the case of an idealized stoss-slope with streamflow divergence will be considered. For this example, the streamlines diverge at a constant angle ϕ over the stoss-side, which is oriented so that the stoss-slope dips towards the oncoming wind with a constant gradient (Tan θ). At the toe of the dune the sand arriving from upwind is q_0 and the initial width of the streamline lane is l_1. The brink is assumed to be oriented perpendicular to the crest, with no curvature. Under such conditions, Equations 1, 2, 3, and 18 indicate that the brink can exist in stable equilibrium with a stoss-side of length x, given by :

$$x = \sqrt{\frac{2q_0 l_1}{\gamma\phi\ K\ \text{Tan}\ \theta}} \tag{24}$$

This regulation of the position of the brink relative to the crest occurs primarily along the dune wings, because the central portions of the brink adjust by change of orientation and curvature (in fact, the flow there may converge slightly, see Figure 2A).

Equation 25 also explains the forward displacement of the brinkline on the lower dunes within a field of barchans. The smaller dunes have lower value of H/W (Finkel, 1959; Hastenrath, 1967), so that both the average stoss-slope, θ, and the flow divergence, ψ, are less, requiring the longer stoss-side (the migration rate of dunes is approximately inversely proportional to crest height, as is the scale width, l_1 while q_0 is presumably uniform).

The adjustment of the dune to variations in the saturation of the oncoming sandflow is less certain, as is the total range of saturation for which barchans are stable. A low saturation implies a greater potential for erosion along the leading edge, resulting in a steeper dune and increased divergence at the leading edge, causing a large W/L ratio. Equation 24 suggests that the brink should lie closer to the leading edge. An open, crescent-moon-shaped dune, which is nearly two-dimensional should result. A whaleback form with a small slip face would probably characterize a barchan with a large saturation.

A change in the direction of the oncoming wind results in greater wind velocities over the more upwind wing and much reduced shear on the sheltered wing (Fig. 13). This causes a more rapid migration of the upwind wing, which will tend to reorient the dune with the wind.

Dune size

Barchan dunes vary from a few meters in width to several hundred meters. A few kilometer-scale barchanoid dunes (for example, the Pur-Pur

dune of Peru and the Alogdones dunes of California) may or may not fall within the size continuum of normal barchans. The factors controlling dune size may either reside in natural scales of atmospheric turbulence or they may be controlled by sand transport processes. Ripple scale appears to be determined by the average path length of sand in saltation (Ellwood et al., 1975), whereas the size of the largest (draas) dunes may be related to large convection cells with wavelengths on the order of the thickness of the atmospheric boundary layer (Wilson, 1972; Hanna, 1969; Wipperman, 1969). The factors controlling the scale of the large class of natural eolian dunes ranging from about 10 to 500 meters in size is much less certain. Wilson (1972) feels that their scale is controlled by transport properties, such as grain size, velocity, and saturation, while Cook and Warren (1973) suggest natural atmospheric scales. The observations of Wilson (1972, Fig. 2) suggest that dune size increases with grain size. Unfortunately, little other systematic data has been collected regarding the relationship between dune scale and such factors as grain size, dominant wind velocity, upwind roughness and saturation of the sandflow. Unlike subaqueous dunes where the flow depth imposes a natural scale; atmospheric boundary layer flows do not have as well-defined a vertical structure. In the surface layer, a zone about 50-200 meters deep in which Coriolis effects are negligible and the shear stress is nearly constant with height (Plate, 1971; Lumley and Panofsky, 1964), the natural scaling factor is the aerodynamic roughness. Most natural dunes are deeply submerged in this layer.

Transport-related scale factors might emerge from two length scales, 1) the distance lag between change of shear stress and response of the saltation load, and 2) upwind roughness length z_0 (or z_{0a}). The

simulation model suggests that the first of these factors is unimportant, except that it sets a minimum size for a stable dune (Bagnold, 1956, p.296). A sand body of the same size or smaller than the distance lag would not have the variance of transport rates necessary to cause the pattern of erosion and deposition necessary for equilibrium. This minimum size is probably proportional to the average path length of grains in saltation, and hence, like ripples, the minimum wavelength would increase with larger grain size and stronger wind shear.

Dune and scale may also be affected by roughness length, because variations in roughness change the pattern of wind shear on the dune. The possible influence of roughness can be illustrated through a heuristic model. In turbulent flow over a low, smoothly-contoured hill the distribution of pressure and wind shear are affected by the upwind roughness, z_0, the dune height, H, and the downwind length, L, of the hill. Numerical simulations of turbulent flow by Taylor and Gent (1974) suggest that the maximum pressure drop, p_H, occurs at the crest of the hill and is related to the geometrical parameters as follows:

$$\frac{p_H}{\rho v_{*0}^2} \approx \frac{H^{5/4}}{L^{1/4} z_0} \tag{25}$$

The ratio of the maximum surface shear at the dune crest, v_{*H}, to the upwind shear, v_{*0}, is independent of roughness:

$$\frac{v_{*H} - v_{*0}}{v_{*0}} \simeq K_2 \left(\frac{H}{L}\right)^{5/4} \tag{26}$$

Flow over a smooth, three-dimensional dune might be expected to respond

variations in H, L, and z_0 in approximately the same manner.

Large and small barchans are nearly geometrically similar, which suggests that the surface flow patterns are likewise similar. Bernoulli's Law indicates that self-similar streamline patterns will occur if the left-hand side of Equation 25 is a constant independent of dune scale. If relative values of sand discharge over the dune were likewise independent of scale, a scale-independent equilibrium pattern of erosion and deposition rates would result. Equal relative discharge rates occur if the ratio of sand discharge at the dune crest, q_H, to the sandflow from upwind, q_0, is independent of dune size. Assuming that the sandflow from upwind is nearly saturated, Bagnold's original transport formula (Equation 7) indicates that the left-hand side of Equation 26 is also constant. These two results imply that dune scale, L, should be proportional to the upwind roughness, z_0, and that the relative dune steepness, H/L, is independent of dune scale. These results seem intuitively reasonable.

If the upwind roughness is controlled by fixed roughness elements, such as the rock cover on the desert floor, or vegetation, then dune size would, if this model is realistic, be larger the greater the upwind roughness. However, no systematic data is available on the correlation between dune size and upwind roughness. Barchanoid dunes on the coastlines between Virginia Beach, Virginia and Cape Hatteras, North Carolina are very large (several hundred meters), and lie downwind from abundant vegetation, a rough foredune topography, and, further upwind, the sea surface, which during strong winds is also rough. Barchanoid dunes on the Navajo Indian Reservation appear to be larger the greater the upwind roughness. Transverse gypsum dunes at White Sands, New Mexico increase in size downwind from a smooth playa lake, due, perhaps, to the form resistance of the

dunes. In the latter case an age-dependent size is an alternative explanation.

If the natural roughness elements are small, and the sandflow is near saturation, the roughness will be controlled by the saltation process, as indicated by Equation 6. This equation, together with Equation 11, relating U_t to grain size, indicate that the upwind roughness increases as u_{*0} increases, but decreases as grain size increases (for a constant upwind shear velocity). Thus, if dune size is proportional to the saltation roughness, grain size and dune scale would be inversely correlated. This is opposite to the direct proportionality observed by Wilson (1971). However, the dominant shear stress for dune formation increases with grain size, due to the greater threshold velocity. Depending upon the natural variation with grain size of the ratio of dominant shear stress to threshold shear, the saltation roughness (and the dune size) might either remain constant or increase as grain size becomes larger.

The elapsed time since initiation of the dune may be an important scale factor. In a field of barchans new dunes appear to originate as small whaleback dunes in the streamers from larger barchans or from the breakup of larger dunes. Due to the inverse relationship between dune height and migration rate (Bagnold, 1941, p.214; Hastenrath, 1967; Coursin, 1964) large barchans are often overtaken by smaller and their merger frequently creates a single dune of larger size. The merger process encourages development of equal-sized dunes which do not collide because of equal rates of movement (Rim, 1958). Thus dune scale may be time dependent. Whether natural atmospheric, roughness, or transport scales impose an upper as well as lower limit to barchan size is at present uncertain.

Pebble ripples, about 20 cm to 25 m in wavelength (Ellwood et al., 1975) are generally barchanoid in shape when they occur in isolation or at the upwind edge of a field of pebble ripples. They may originate by a mechanism similar to that of barchan dunes, with gain of creep-load pebbles from upwind balanced by streamer loss at the tails. The granules are propelled primarily by the impact of the finer saltating component and, to a less extent, by wind stress. Because of the rolling motion, the granules are deposited on the sheltered slip face, whereas the bulk of the saltating grains rebound over the lee-side reverse eddy. Because both the wind stress and density of grain impact increase with height, an equilibrium form similar to barchans results. Downwind in pebble ripple fields the crestlines become nearly straight and perpendicular to the wind (subaqueous analogs are cited by Allen, 1968, p. 91). Downwind development of a self-regulating resonance between saltation paths and the ripple form is the most likely explanation for the stability of the two-dimensional form, such that each ripple has the same migration rate and negligible pebble supply from upwind. The scale of pebble ripples appears to be controlled by the average path length of the saltating grains (Ellwood et al., 1975).

CONCLUSIONS - RESEARCH NEEDS

If the interactions between sand transport, dune form and fluid flow could be completely modeled, the limits of stability of the dune and the factors determining the form and size of the dune could be readily determined and extended to extraterrestrial environments. Ideally, such a theoretical model should first predict the details of the air flow over any three-dimensional sand deposit protruding from a level desert surface, in particular, the streamline pattern near the surface and the shear stress distribution, given, say an undisturbed logarithmic boundary layer upstream from the obstacle. Then, using appropriate bed-load transport equations, the obstacle would be modifed by erosion and deposition in a simulation model. The simulation would procede by small steps to an equilibrium form (if, indeed, one is established), If a barchan form developed, the simulation could then investigate the effects of variation in velocity of the oncoming winds, in quantity of supplied sand, in roughness length, in grain size, and in constancy of wind direction, as well as scaling to conditions on other planets. Unfortunately, theoretical modeling of fluid flow around three-dimensional objects with arbitrary boundary conditions, while conceptually feasible, requires extensive computations. The authors are presently attempting to develop an efficient computer simulation model. If this is not possible, simplified quasi-two-dimensional models will be tried.

A parallel need exists for comprehensive field measurements. Detailed measurement of sand flow (total quantity, grain size and vertical distribution) and the associated velocity profiles at many points on and upwind from barchan dunes would help to refine the model presented here.

ACKNOWLEDGEMENTS

Lunar and Planetary Programs, supported by the National Aeronautics and Space Administration, Contract NGR-47-005-172. The manuscript was substantially improved as a result of comments by George Hornberger.

Table 1. Values of fixed parameters

Parameter	Value
B	.017
C	1.8
C'	4.2
C"	5.0
D (cm)	.025
F ($cm^{\frac{1}{2}}/sec$)	3,300
g (cm^2/sec)	980
ρ (g/cm^3)	.0012
σ (g/cm^3)	2.65
α (degrees)	30.5

Table 2 Comparison of simulated stoss-side erosion and deposition rates with observed and predicted rates.

Transport[5] Path	Slope[6] Effect	Delay (λ)	Convergence[2]	Correlation Coefficients with[3] Observed[1]	Predicted	Bias with[3] Observed	Predicted	Variance with[3] Observed	Predicted	P1[4]	P2
				A. Single Simulations							
W	S	0	C	.56	.59	-.013	.0002	.0052	.0052		
R	S	0	C	.48	.47	-.0043	.0093	.0070	.0077		
W	N	0	C	.69	.71	-.011	.0023	.0044	.0042		
R	N	0	C	.65	.62	-.0013	.012	.0048	.0055		
W	S	1	C	.45	.49	-.012	.0016	.0050	.0053		
W	N	0	X	.69	.66	-.0098	.0038	.0037	.0043		
Observed Rates Versus Predicted				--	.87	--	-.014	--	.0015		
				B. Least-squares Linear Combinations of Simulations							
W	S	0	C	.56	.59	-.011	.0006	.0052	.0052	79	93
R	S	0	C								
W	N	0	C	.72	.72	-.0066	.0056	.0036	.0038	53	67
R	N	0	C								
W	N	0	C	.70	.71	-.010	.0029	.0036	.0040	23	58
W	N	0	X								

Table 2 (continued)

Explanation:

[1] Observed rates from field observations (Fig. 4A). Predicted rates from assumption of equilibrium during translation (Fig. 4B). Simulations assume 50% initial saturation, $V_o'(80)$ = 1000 cm/sec, and a grain size of .25 mm.

[2] C = Convergence term in Equation 1 is retained.

X = Convergence effects in Equation 1 are ommitted.

[3] 285 data points from stoss-side used in calculation of results.

[4] P1 = Percent weighting of first model listed in least-squares prediction of observed erosion and deposition rates.

P2 = Percent weighting of first model listed in least-squares prediction of predicted erosion and deposition rates.

[5] W = Assumed transport following wind streamlines.

R = Assumed transport following ripple train.

[6] N = Direct slope effects upon transport discounted (Equations 7-9).

S = Slope effects on transport given by Equation 14.

Table 3. Correlations of simulated velocity distributions with the velocity measurements in the field and laboratory.[1]

Transport[3] Path	Transport[4] Law	Saturation (%)	Slope[5] Effect	Correlation Coefficients with[2] Field Velocities	Laboratory Velocities
W	M.B.	50	N	.52	.78
"	"	"	S	.60	.83
"	"	100	N	.51	.77
"	"	"	S	.61	.82
R	O.B.	50	N	.38	.69
"	"	"	S	.54	.85
"	M.B.	50	N	.54	.74
"	"	"	S	.64	.84
"	"	100	N	.57	.78
"	"	"	S	.63	.84

Explanation:

[1] All simulations assume V(80) = 100 cm/sec; d = .25 mm; zero delay.

[2] Thirteen data pairs in each correlation. Correlation coefficient between field and and laboratory velocities is .77.

[3] W = Assumed transport following wind streamlines

R = Assumed transport following ripple train

[4] M.B. = Modified Bagnold transport law (Equation 9).

O.B. = Original Bagnold transport law (Equation 7).

[5] N = Direct slope effects upon transport discounted (Equations 7-9).

S = Slope effects on transport given by Equation 14.

REFERENCES

Allen, J.R.L. (1968) Current Ripples, Their Relation to Patterns of Water and Sediment Motion. North Holland, Amsterdam, 433 p.

Bagnold, R.A. (1941) The Physics of Blown Sand and Desert Dunes. Methuen, London, 264 p.

_____ (1956) Flow of cohesionless grains in fluids. Trans. Royal Soc. London, 249, 235-297.

_____ (1973) The nature of saltation and of 'bed-load' transport in water. Proc. Royal Soc. London, 332A, 463-504.

Blom, J. and Wartena, L. (1969) Influence of changes in surface roughness on the development of the turbulent boundary layer in the lower layers of the atmosphere. J. Atm. Sci., 26, 255-265.

Chepil, W.S. (1945) Dynamics of wind erosion: II. initiation of soil movement. Soil Sci. 60, 397-411.

_____ and Milne, R.A. (1941) Wind erosion of soil in relation to roughness of surface. Soil Sci. 52, 417-433.

_____ and Woodruff, N.P. (1963) The physics of wind erosion and its control. Adv. in Agronomy, 15, 211-302.

Cooke, R.V. and Warren, A. (1973) Geomorphology in Deserts. U. Calif. Press, Berkeley, Part 4.

Coursin, A. (1964) Observations et expériences faites en avril et mai 1956 sur les barkhanes du Souehel el Abiodh (region est de Port-Étienne). Bull. Inst. Francais D'Afrique Noir, 26A, 989-1022.

Elliot, W.P. (1958) The growth of the atmospheric internal boundary layer. Trans. Am. Geophys. Union, 39, 1048-1054.

Ellwood, J.M., Evans, P.D., and Wilson, I.G. (1975) Small scale eolian bedforms. Journ. Sed. Petrology, 45, 554-561.

Finkel, H.J. (1959) The barchans of southern Peru. J. Geology, 67, 614-647.

Gad-el-Hak, M., Pierce, D., Howard, A., and Morton, J.B. (1976) Interactions of unidirectional winds with an isolated barchan sand dune. Tech. Rept., Univ. of Virginia, Charlottesville.

Greeley, R., Iverson, J.D., Pollack, J.B., Vdovich, N., and White, B.R. (1974) Wind tunnel studies of Martian eolian processes. Proc. Royal Soc. London, 341A, 331-360.

Hanna, S.R. (1969) The formation of longitudinal sand dunes by large helical eddies in the atmosphere. J. Appl. Met., 8, 874-883.

Hastenrath, S.L. (1967) The barchans of the Arequipa region, southern Peru. Zeit. für Geom., 11, 300-311.

Howard, A.D. (in press) Effect of slope on the threshold of motion and its application to orientation of wind ripples. Bull. Geol. Soc. Am.

Iverson, J.D., Pollack, J.B., Greeley, R., and White, B.R. (1976) Saltation threshold on Mars: the effect of interparticle force, surface roughness, and low atmospheric density. Icarus, 29, 381-393.

Kennedy, J.F. (1969) The formation of sediment ripples, dunes, and antidunes. Ann. Rev. Fluid Mech. 1, 147-169.

Kokus, M.T. (1975) A physical model of the Earth's atmospheric boundary layer. Thesis, Univ. of Virginia, unpublished.

Lettau, K. and Lettau, H. (1969) Bulk transport of sand by the barchans of the Pampa de La Joya in southern Peru. Zeit. für Geomorphology, 13, 182-195.

_____ (in press) Experimental and micrometeorological field studies of dune migration. In: Exploring the World's Driest Climate (Ed. by Lettau, K. and Lettau, H.), Univ. Wisconsin Press, Madison.

Long, J.T. and Sharp, R.P. (1964) Barchan-dune movement in the Imperial Valley, California. Bull. Geol. Soc. Am., 75, 149-156.

Lumley, J.L. and Panofsky, H.A. (1964) The Structure of Atmospheric Turbulence. John Wiley, New York, 239 p.

Merrit, F.S. (1968) Structural theory. In: Standard Handbook for Civil Engineers (Ed. by Merrit, F.S.) McGraw-Hill, New York, ch. 6.

Norris, R.M. (1966) Barchan dunes of Imperial Valley, California. J. Geology, 74, 292-306.

Plate, E.J. (1971) Aerodynamic Characteristics of Atmospheric Boundary Layers. A.E.C. Critical Review Series, 190 p.

Rao, K.S., Wyngaard, J.C., and Coté, O.R. (1974) The structure of the two-dimensional internal boundary layer over a sudden change of surface roughness. J. Atm. Sci., 31, 738-746.

Raudkivi, A.J. (1966) Bed forms in alluvial channels. J. Fluid Mech., 26, 507-514.

Reynolds, A.J. (1965) Waves on the erodible bed of an open channel. J. Fluid Mech., 22, 113-133.

Rim, M. (1958) Simulation, by dynamical model, of sand tract morphologies occurring in Israel. Bull. Res. Council of Israel, 7G, 123-136.

Schlicting, H. (1968) Boundary Layer Theory. McGraw-Hill, New York, 747 p.

Smith, R.S.U. (1970) Migration and wind regime of small barchan dunes within the Algodones dune chain, Imperial county, California. Dissertation, Univ. Arizona, unpublished.

Taylor, P.A. and Gent, P.R. (1974) A model of atmospheric boundary-layer flow above an isolated two-dimensional 'hill'; an example of flow above 'gentle topography'. Boundary-Layer Met. 7, 349-362.

Williams, G. (1964) Some aspects of the eolian saltation load. Sedimentology, 3, 257-287.

Wilson, I.G. (1971) Desert sandflow basins and a model for the development of ergo. Geog. J., 137, 180-197.

_____ (1972) Aeolian bedforms--their development and origins. Sedimentology 19, 173-210.

Wipperman, F. (1969) The orientation of vortices due to instability of the Ekman-boundary. Beitr. zur Physik der Atm., 42, 225-244.

Yalin, M.S. (1971) Theory of Hydraulic Models. Macmillan, London, 266 p.

Zingg, A.W. (1953) Wind-tunnel studies of the movement of sedimentary material. Proc. 5th Hydraulic Conf., Iowa State Univ., 111-135.

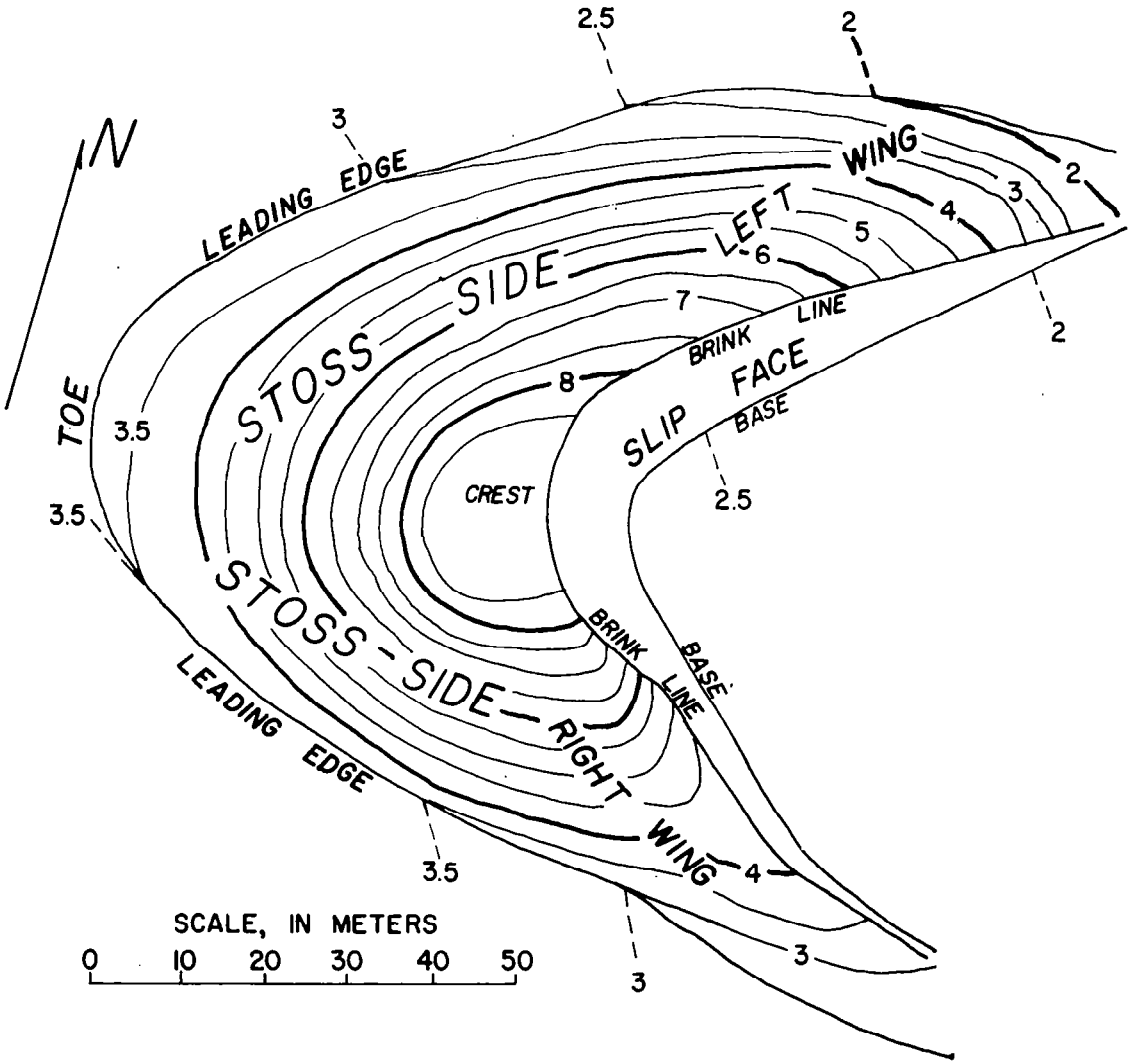

Figure 1.- Topographic map of the prototype barchan dune near the Salton Sea, California, with terminology.

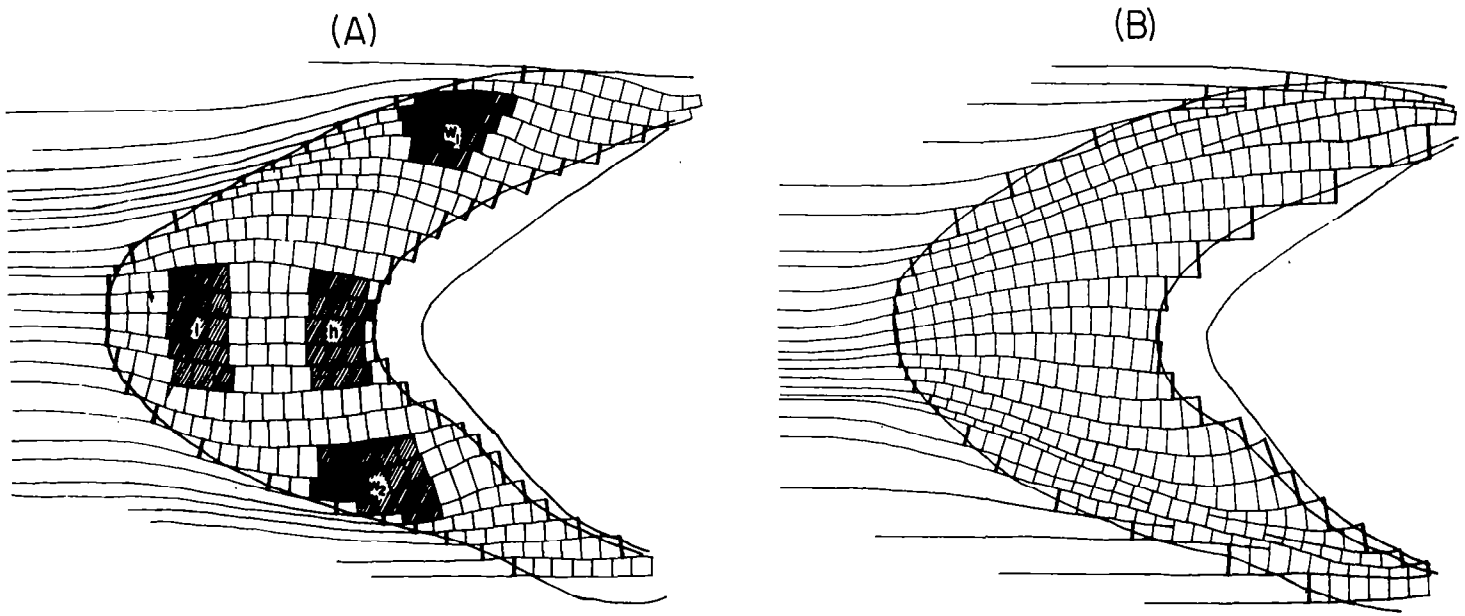

Figure 2.- Transport streamline maps, showing division of streamline lanes into cells. Heavy lines define upwind boundary of leading edge cells and downwind end of brinkline cells: (A), Transport assumed to follow the near-surface wind. Shaded areas discussed in text; (B), Transport assumed to move perpendicular to ripple crests.

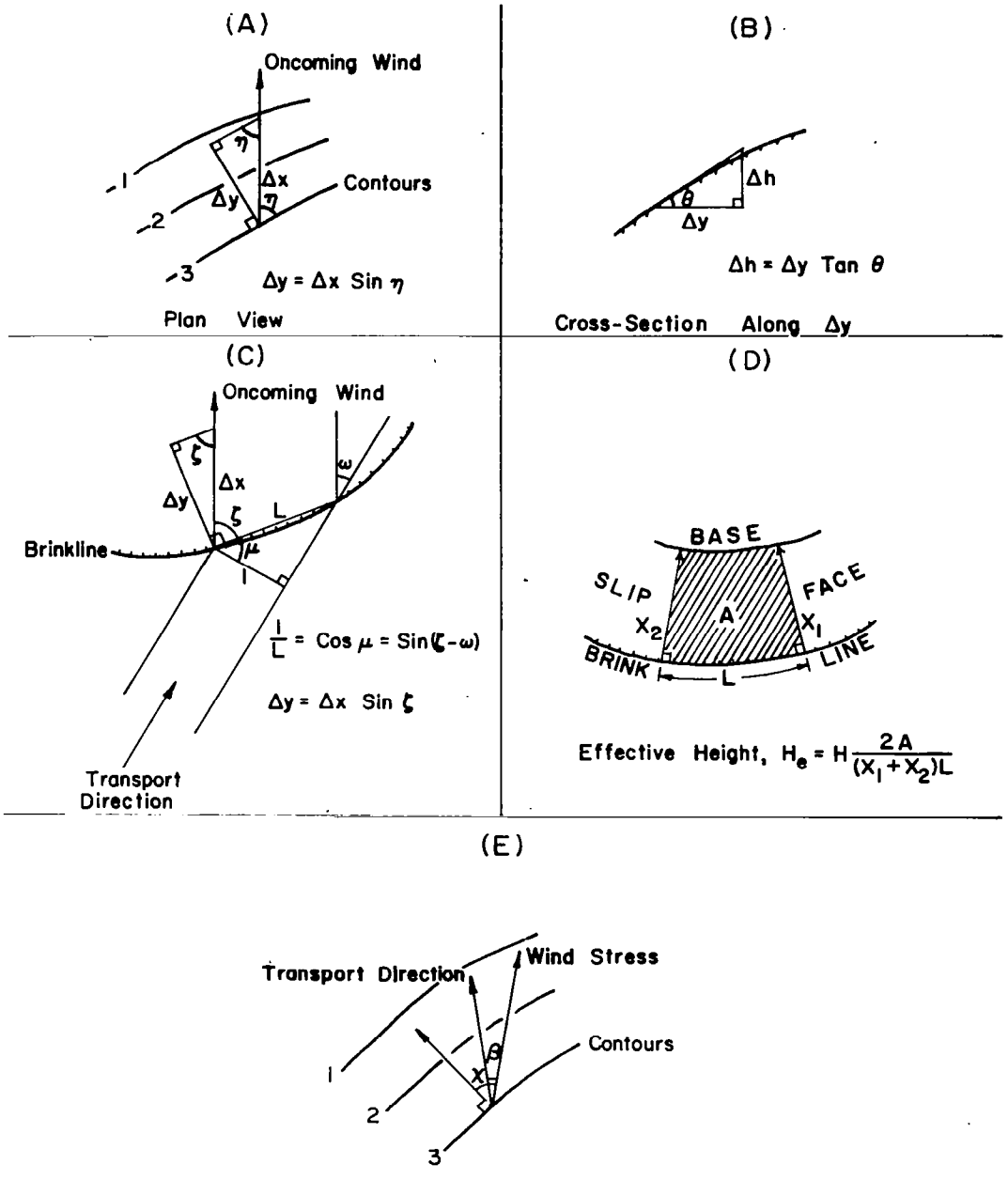

Figure 3.- Geometrical relationships and definitions: (A and B), stoss-side equilibrium; (C and D), crestline equilibrium: (E), deflection of transport direction from direction of applied stress.

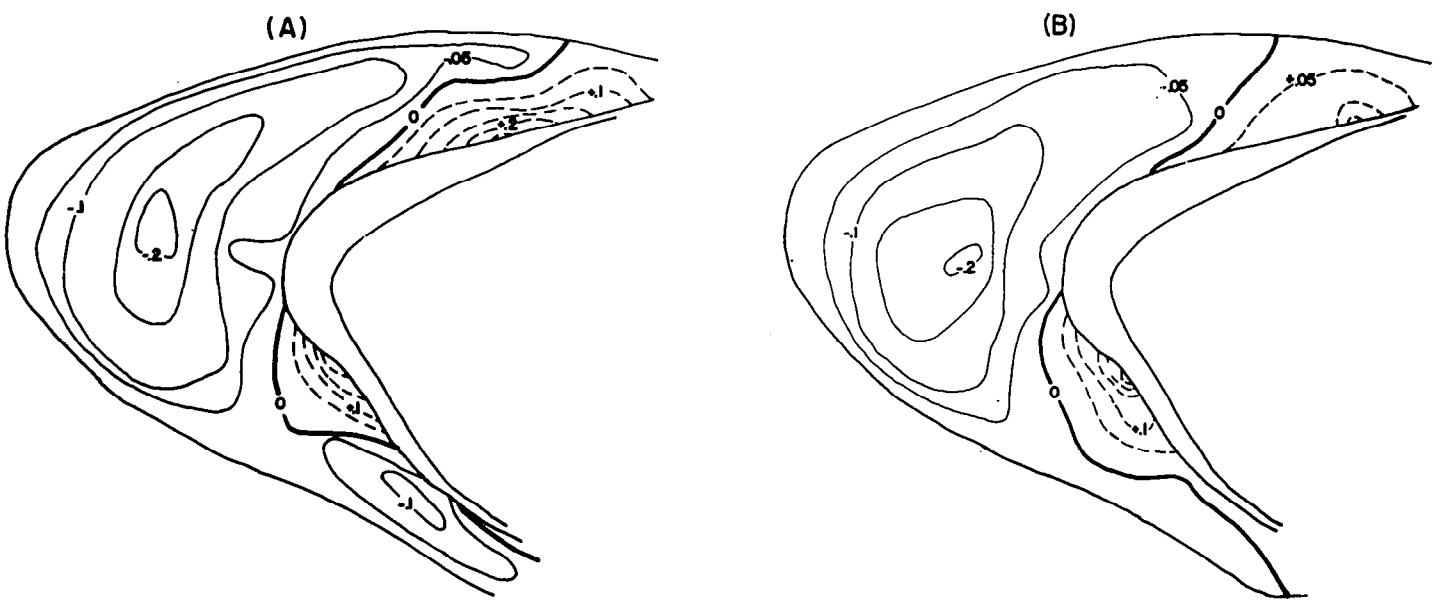

Figure 4.- Scaled erosion and deposition rates on prototype barchan. Solid contours indicate erosion, dashed show deposition: (A), Rates observed during two-week period in field on prototype barchan; (B), Rates predicted by assumption of translation without change of size or shape in directions of dominant wind.

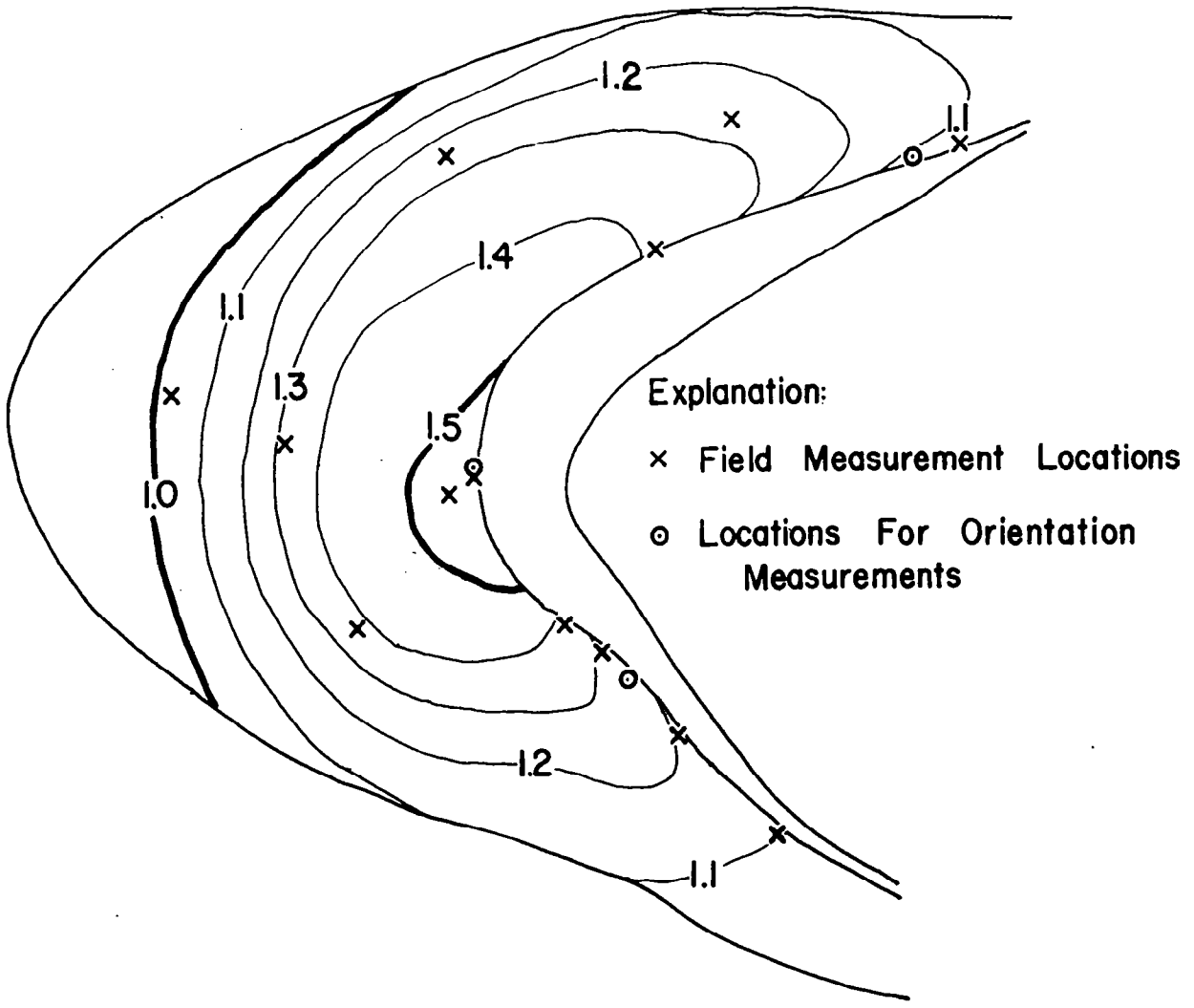

Figure 5.- Contours of velocity measured over model dune. Contours show value of $v(80)/v_0(80)$.

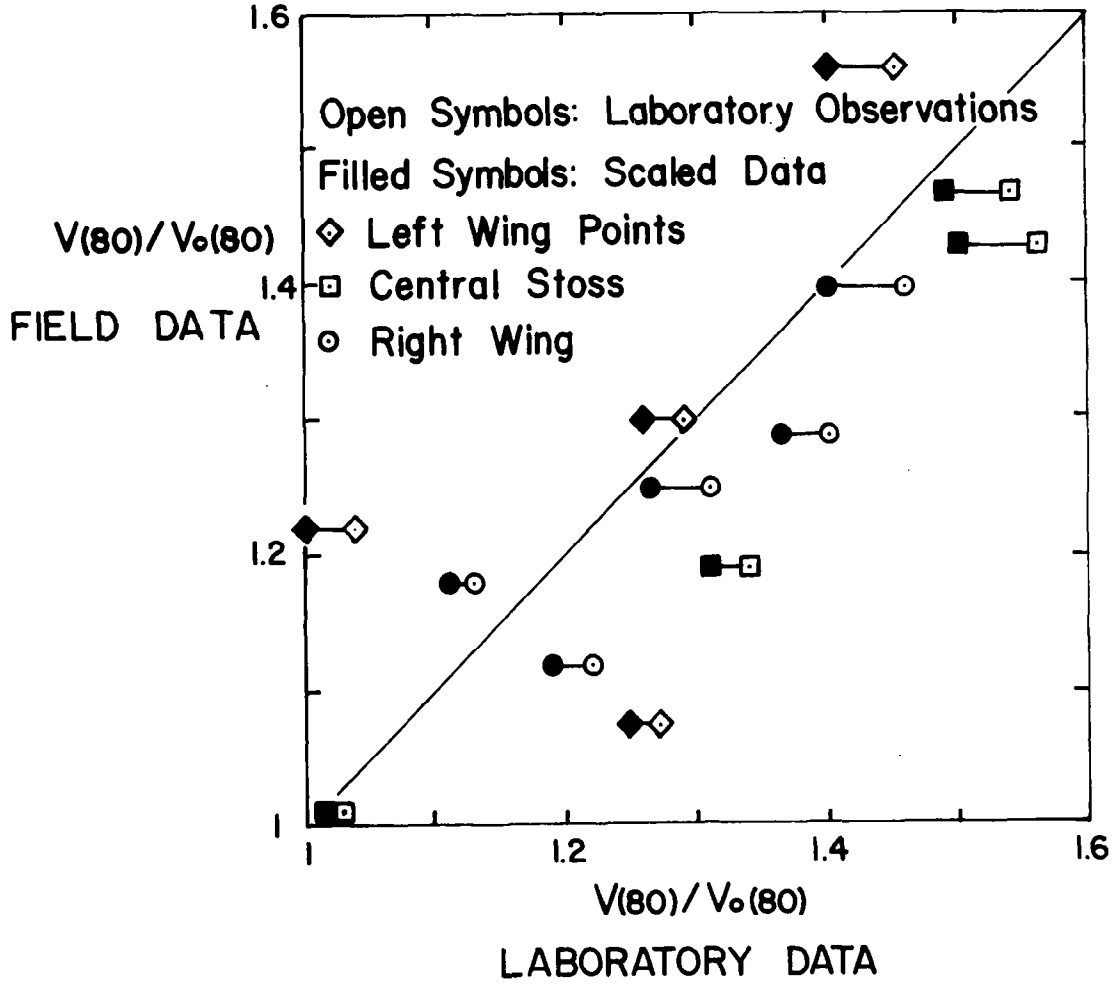

Figure 6.- Relationship between velocities measured in field and over model dune at equivalent heights. Filled symbols show scaling of laboratory data to eliminate bias.

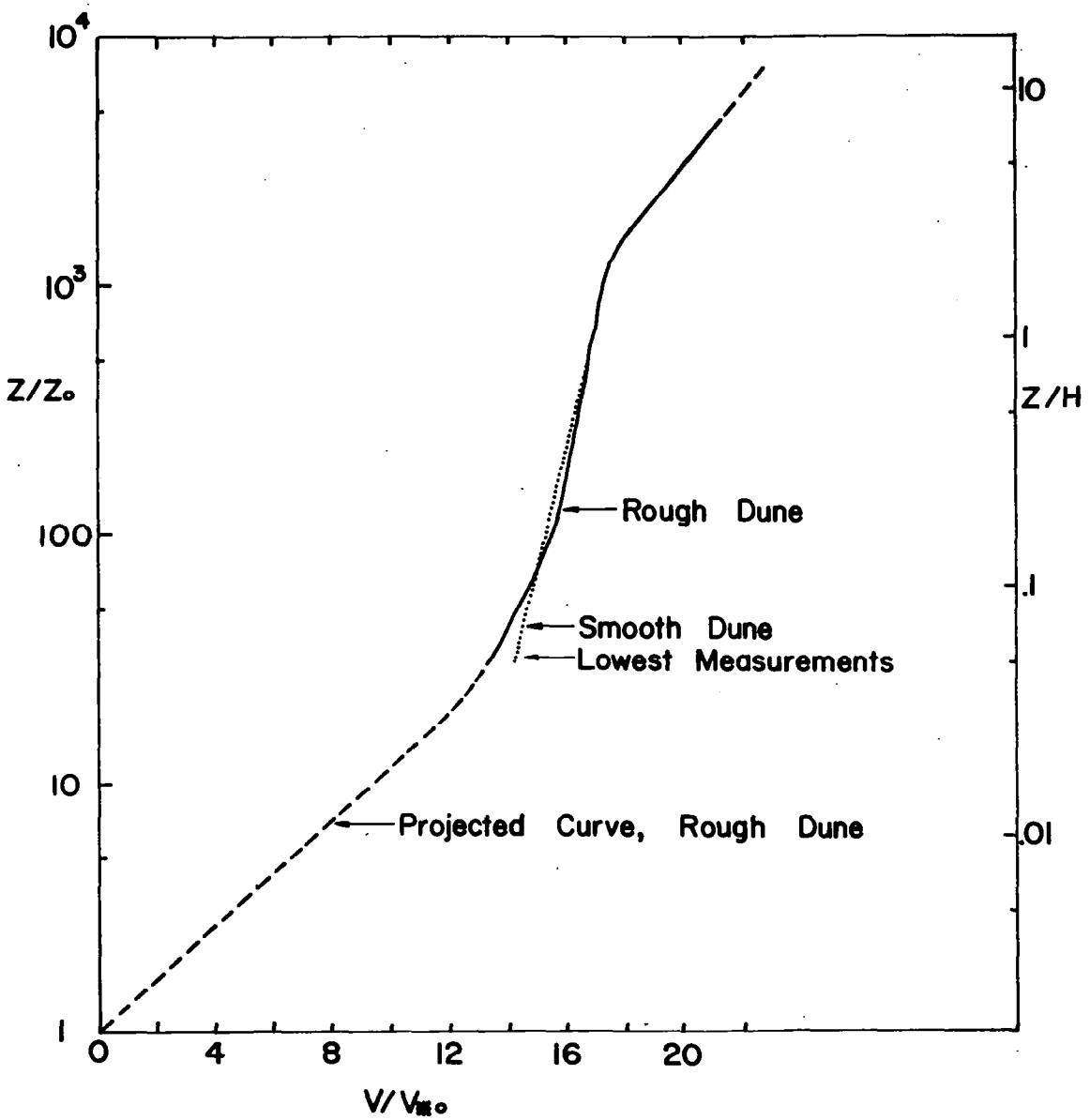

Figure 7.- Velocity profile over center of brinkline, showing acceleration of near-surface flow. Based on laboratory measurements over rough and hydraulically smooth model dunes.

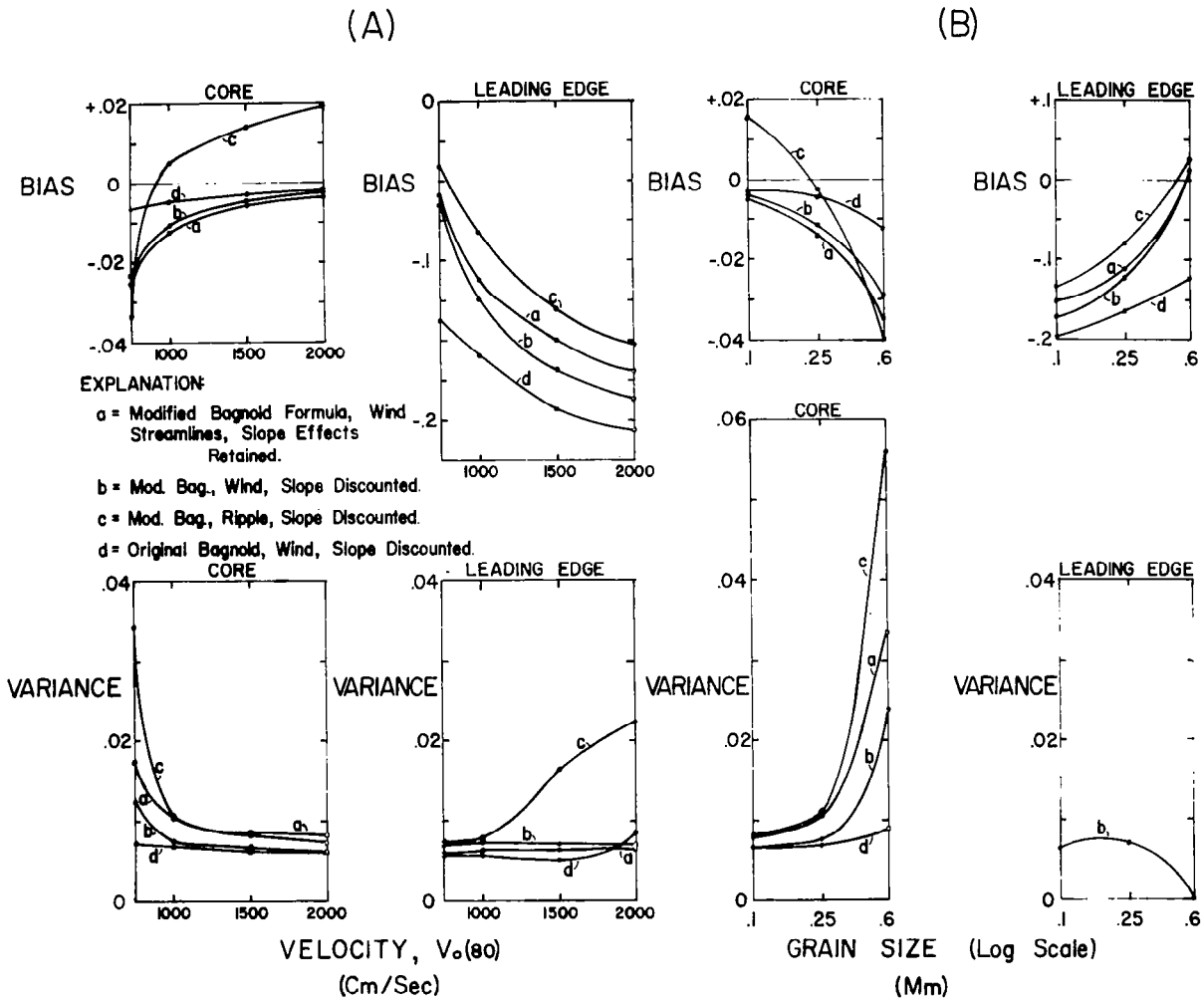

Figure 8.- Effect of velocity (A) and grain size (B) upon the bias and variance of simulated erosion and deposition rates for core (285 cells, wind streamlines and 326 cells, ripple streamlines) and leading edge cells (26 cells, wind streamlines and 24 cells, ripple streamlines).

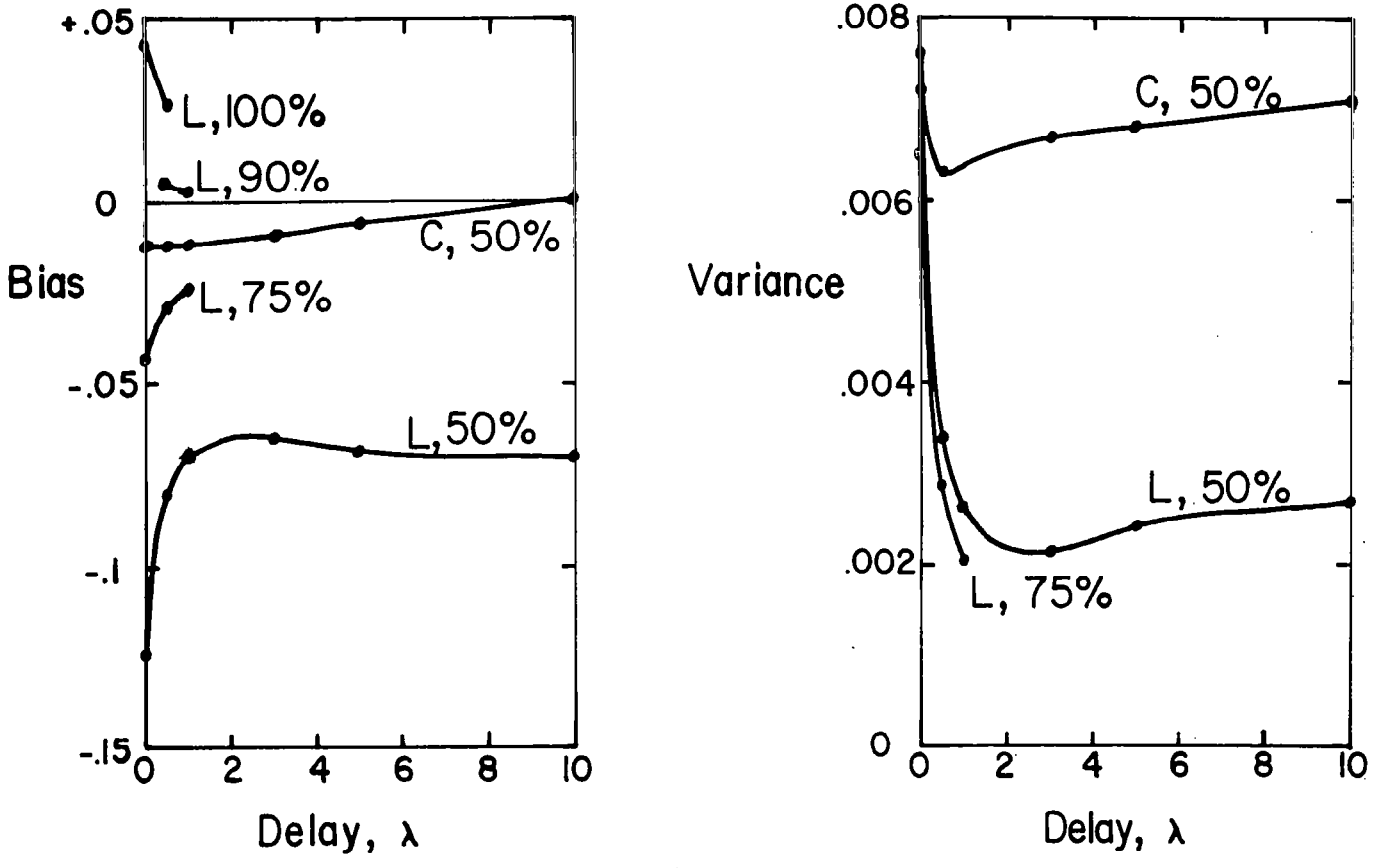

Figure 9.- Effect of delay and percent saturation upon bias and variance, for otherwise nominal conditions.

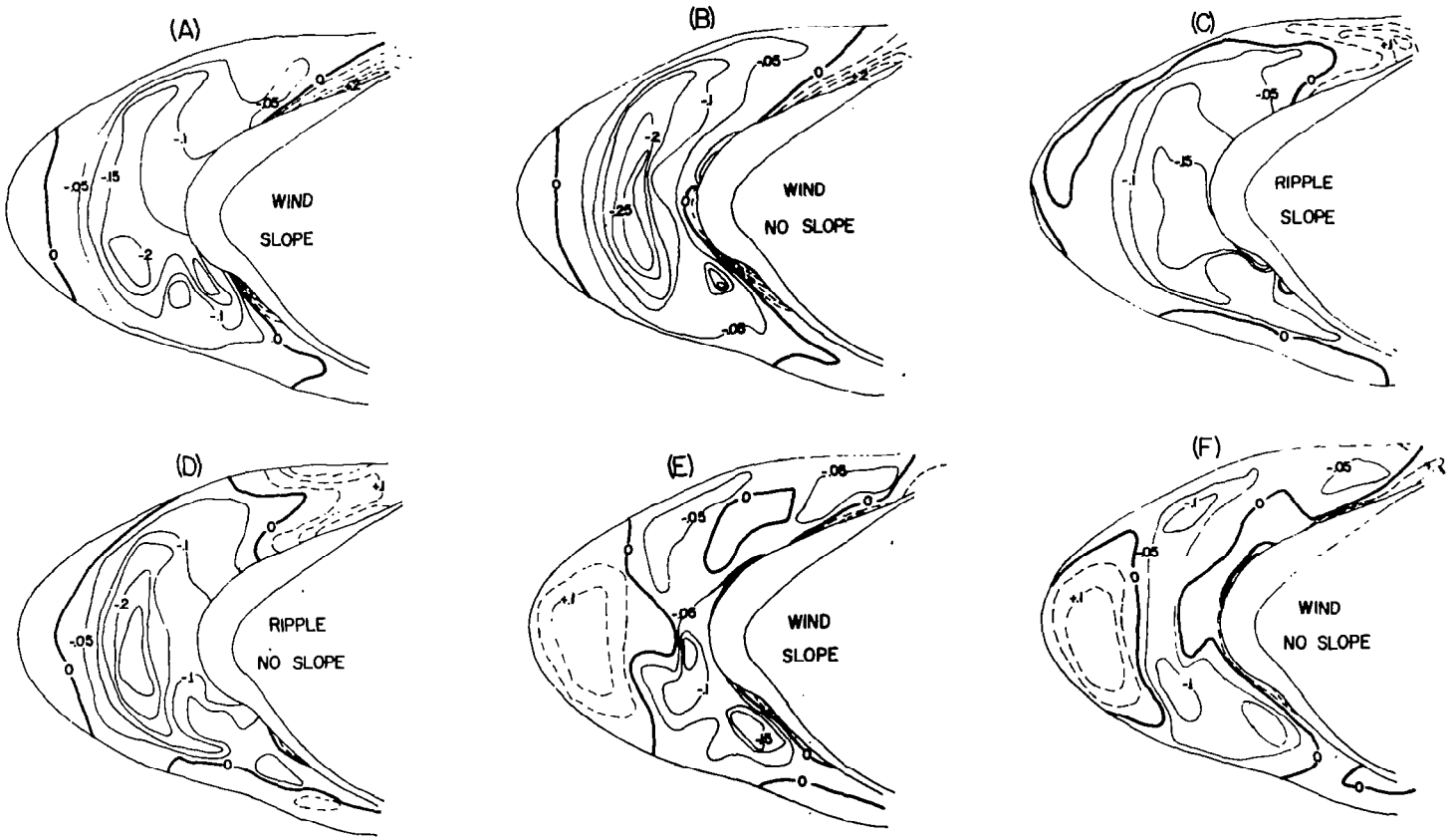

Figure 10.- Simulated erosion and deposition rates (scaled): (A-D), Simulations for nominal conditions except as indicated: Wind = transport following wind streamlines; Ripple = transport along ripple streamlines; Slope = slope effects upon transport included; No Slope = slope effects discounted; (E and F), Differences between simulated erosion rates and rates predicted by assumption of equilibrium.

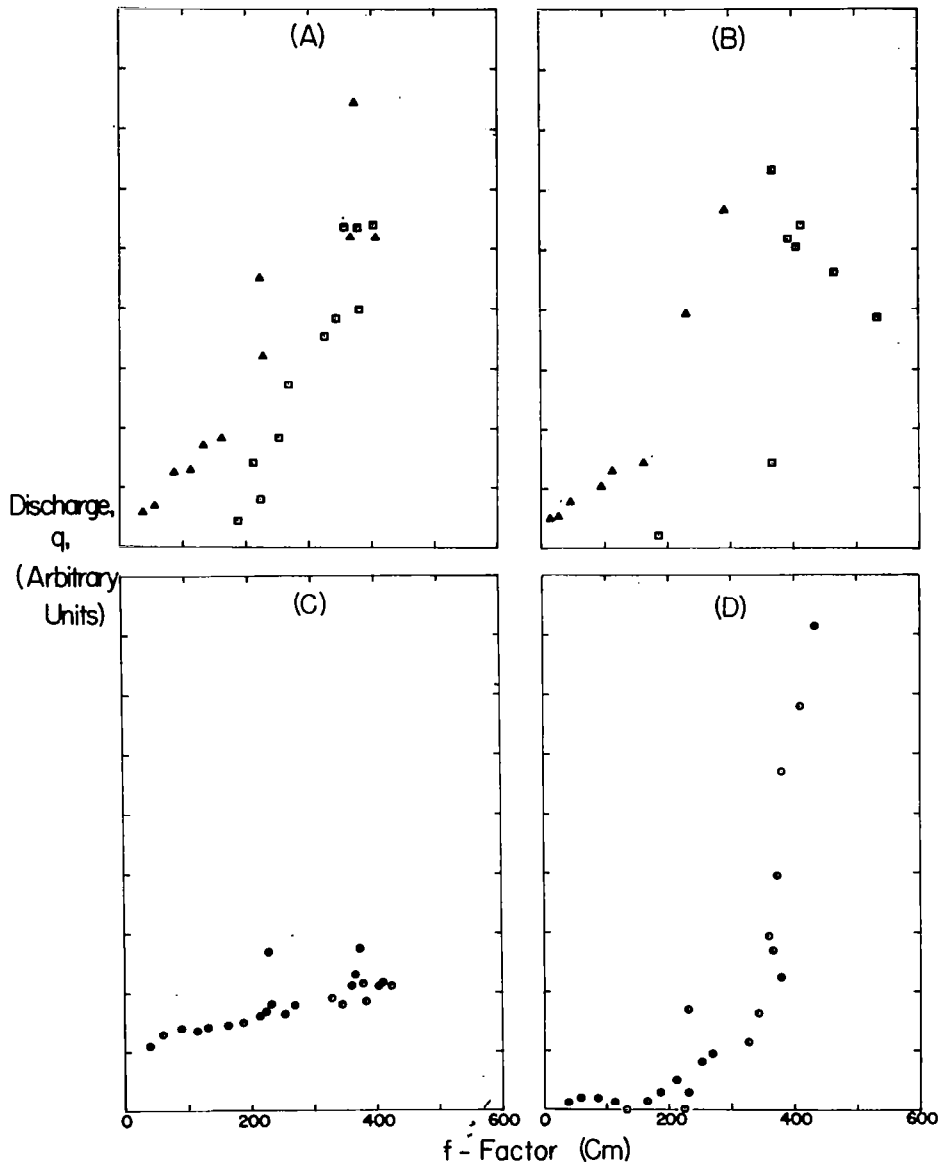

Figure 11.- Relationship between discharge and brink factor, f, for streamline cells terminating on the brinkline. Simulations for nominal conditions except as follows: (A), Transport following wind streamlines; (B), Transport following ripple streamlines; (C), Transport following wind streamlines, average delay of 10 cells, saturation of 50%; (D), Discharges predicted from assumption of equilibrium, transport following wind streamlines; (Squares: left-wing streamline lanes; Triangles: right-wind lanes; Circles: undifferentiated.)

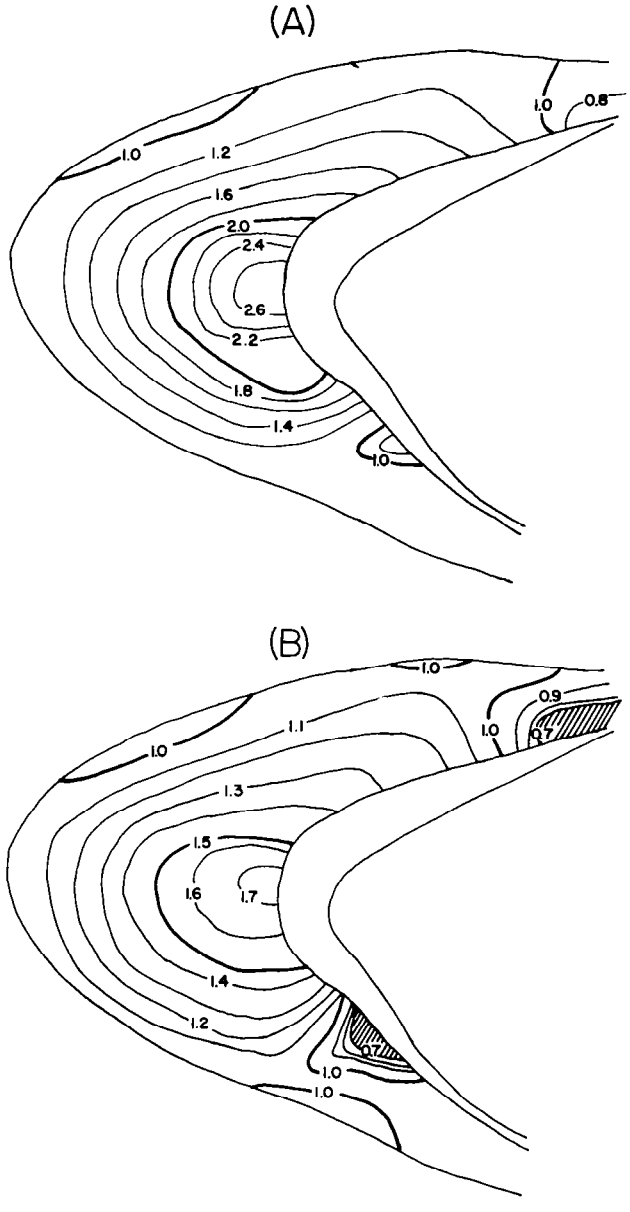

Figure 12.- Velocities ($v(80/v_0(80))$ necessary to produce predicted erosion rates for unidirectional wind: (A), simulation following wind streamlines with slope effects retained; (B), same except slope effects discounted. Hatched areas indicate regions where amount of sediment in trasport is insufficient to match predicted erosion rates.

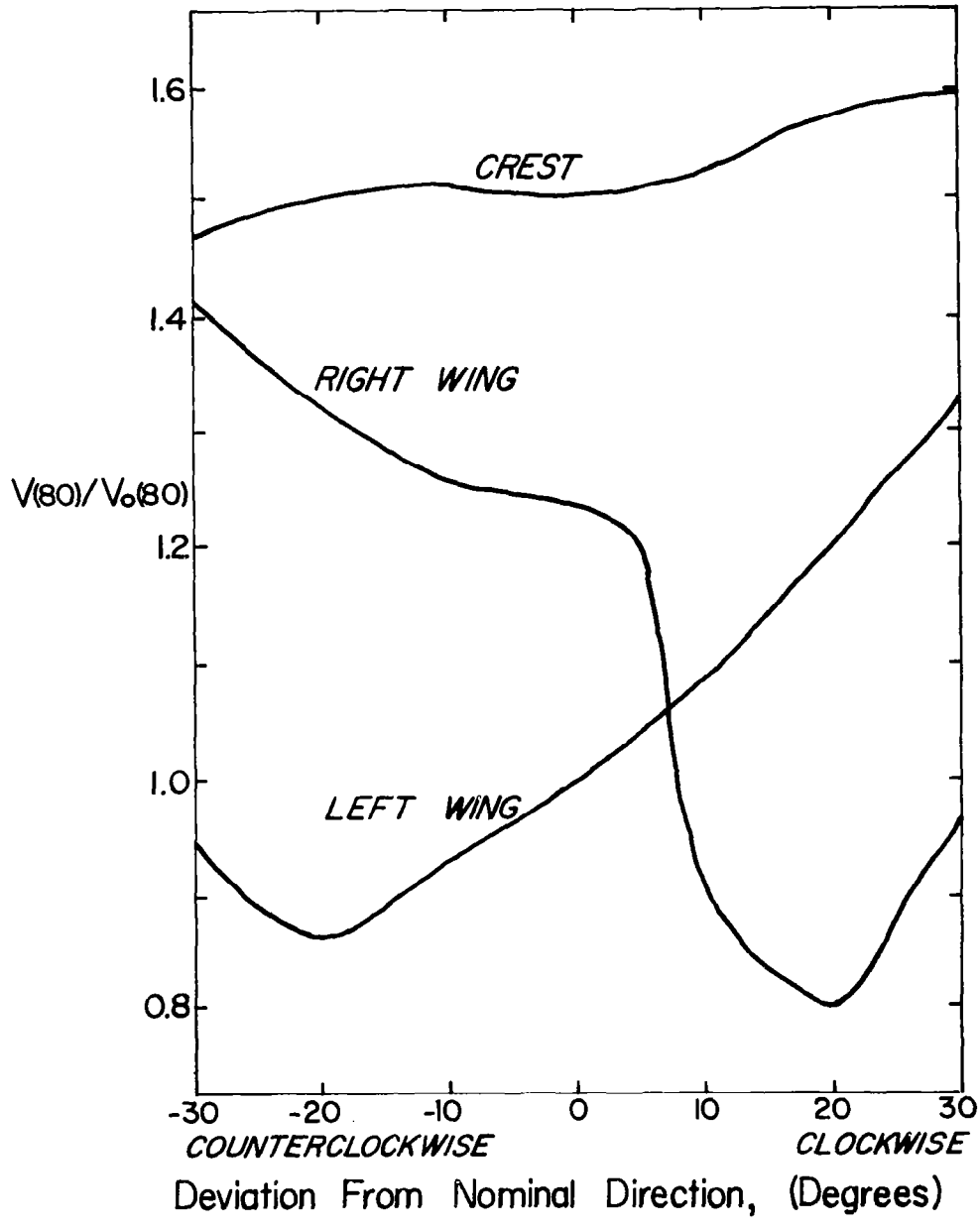

Figure 13.- 0. Effect of variation in direction of oncoming wind upon velocities ($v(80)/v_0(80)$) measured at three brinkline locations on the model dune (see Fig. 5).

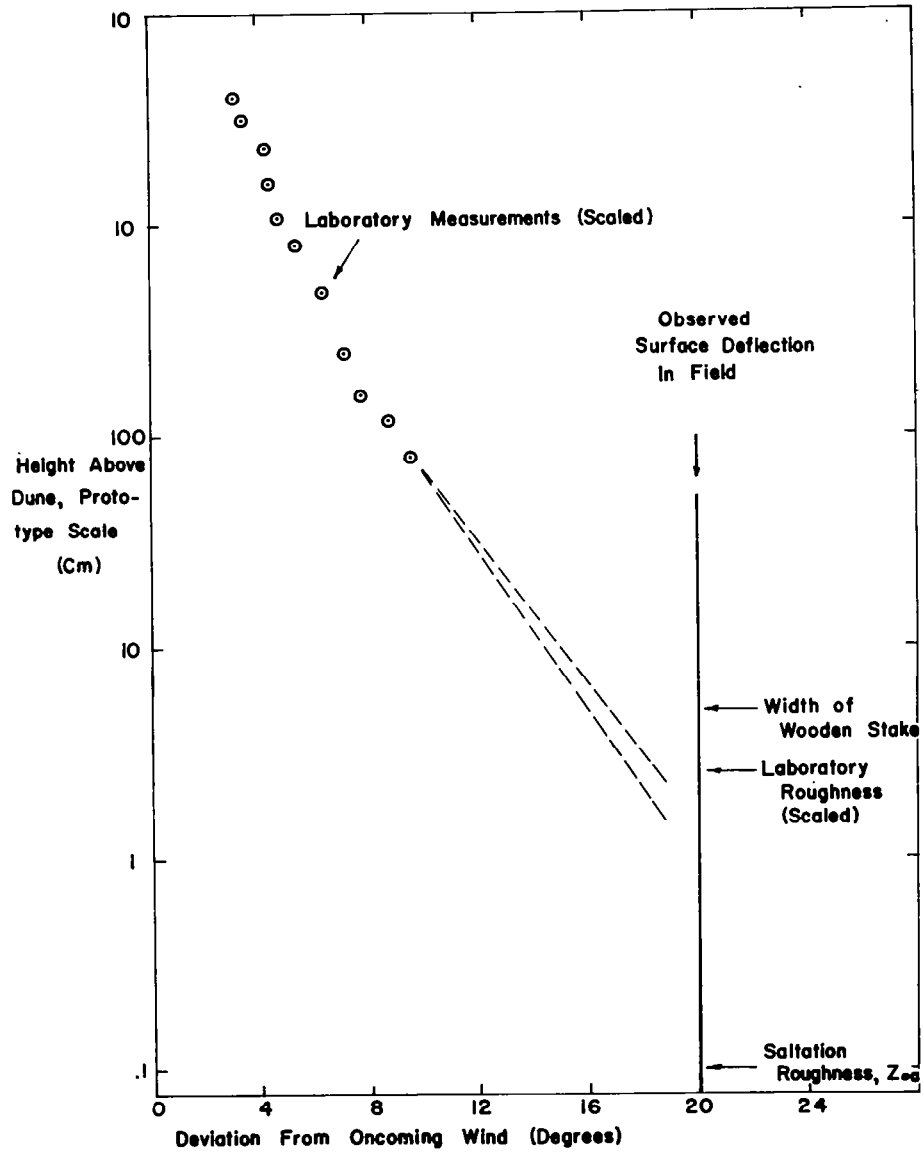

Figure 14.- Deflection of the wind over the dune from the direction of the oncoming wind. Laboratory measurements made on left wind near brink (at circle on Figure 5). Deflection decreases logarithmically with height. Field value of deflection probably has a scale height of about the width of the stake producing the scourmark indicating the wind direction, which also is approximately equal to the average height of saltation. Lack of exact projection of laboratory measurements to the field value is probably due to measurement errors, a difference in direction of the oncoming wind, or slight discrepancy in geometry between prototype and model dunes.

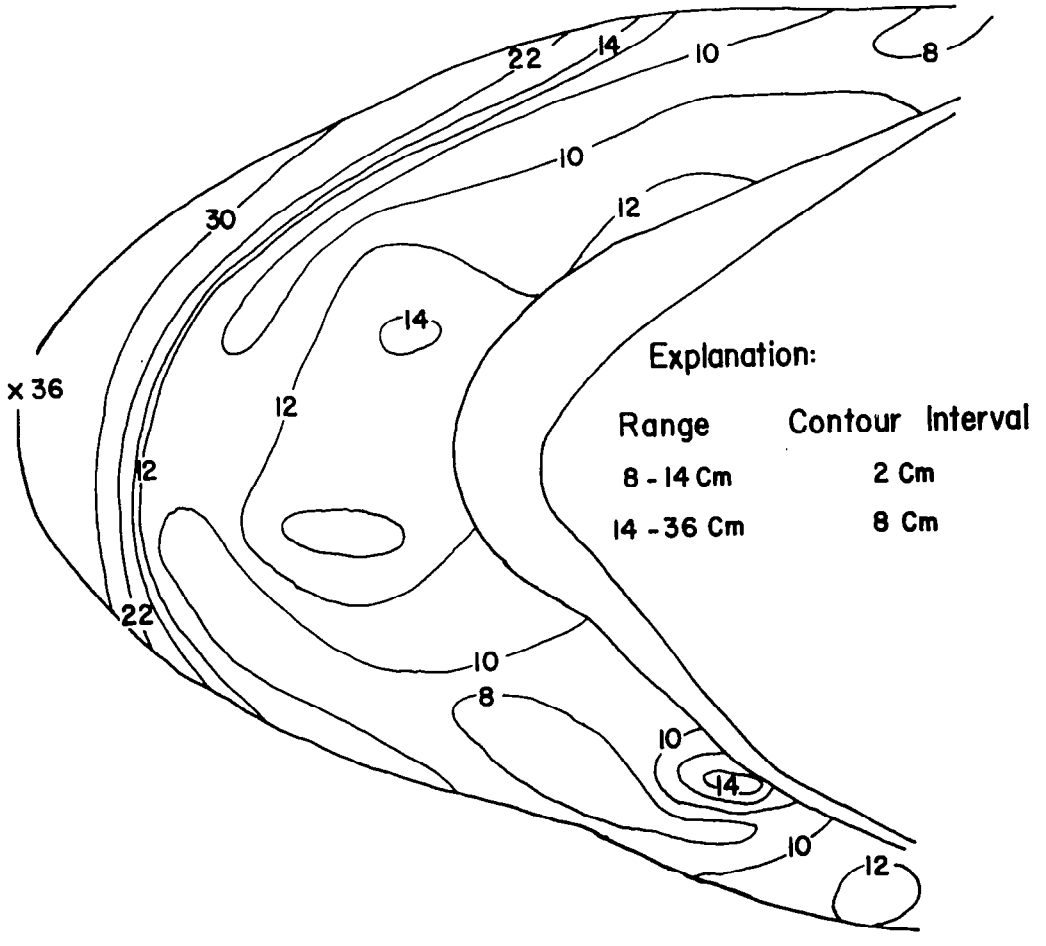

Figure 15.- Wavelength of ripples observed on the prototype barchan (note variable contour interval). Zone of long-crested, granule ripples occurs on toe of leading edge.